

## 11. SITE 1083<sup>1</sup>

### Shipboard Scientific Party<sup>2</sup>

#### HOLE 1083A

**Position:** 20°53.6841'S, 11°13.0720'E  
**Start hole:** 1515 hr, 17 September 1997  
**End hole:** 0225 hr, 18 September 1997  
**Time on hole:** 21.17 hr  
**Seafloor (drill pipe measurement from rig floor, mbrf):** 2189.7  
**Total depth (drill pipe measurement from rig floor, mbrf):** 2391  
**Distance between rig floor and sea level (m):** 11.6  
**Water depth (drill pipe measurement from sea level, m):** 2178.1  
**Penetration (mbsf):** 201.3  
**Coring totals:**  
Type: APC  
Number: 22  
Cored: 201.3 m  
Recovered: 185.32 m (92.06%)  
**Lithology:**  
Unit I: clayey nannofossil ooze

#### HOLE 1083B

**Position:** 20°53.7004'S, 11°13.0738'E  
**Start hole:** 0225 hr, 18 September 1997  
**End hole:** 2210 hr, 18 September 1997  
**Time on hole:** 19.75 hr  
**Seafloor (drill pipe measurement from rig floor, mbrf):** 2194.7  
**Total depth (drill pipe measurement from rig floor, mbrf):** 2397  
**Distance between rig floor and sea level (m):** 11.6  
**Water depth (drill pipe measurement from sea level, m):** 2183.1  
**Penetration (mbsf):** 202.3  
**Coring totals:**  
Type: APC  
Number: 22  
Cored: 202.3 m  
Recovered: 206.41 m (102.03%)  
**Lithology:**  
Unit I: clayey nannofossil ooze

#### HOLE 1083C

**Position:** 20°53.7138'S, 11°13.0734'E  
**Start hole:** 2210 hr, 18 September 1997  
**End hole:** 2310 hr, 18 September 1997  
**Time on hole:** 1.00 hr  
**Seafloor (drill pipe measurement from rig floor, mbrf):** 2190.5  
**Total depth (drill pipe measurement from rig floor, mbrf):** 2200  
**Distance between rig floor and sea level (m):** 11.6  
**Water depth (drill pipe measurement from sea level, m):** 2178.9  
**Penetration (mbsf):** 9.5  
**Coring totals:**  
Type: APC  
Number: 1  
Cored: 9.5 m  
Recovered: 9.78 m (102.95%)  
**Lithology:**  
Unit I: clayey nannofossil ooze

#### HOLE 1083D

**Position:** 20°53.7138'S, 11°13.0734'E.  
**Start hole:** 2310 hr, 18 September 1997  
**End hole:** 1900 hr, 19 September 1997  
**Time on hole:** 19.83 hr  
**Seafloor (drill pipe measurement from rig floor, mbrf):** 2189.9  
**Total depth (drill pipe measurement from rig floor, mbrf):** 2386  
**Distance between rig floor and sea level (m):** 11.6  
**Water depth (drill pipe measurement from sea level, m):** 2178.3  
**Penetration (mbsf):** 196.1  
**Coring totals:**  
Type: APC  
Number: 21  
Cored: 196.1 m  
Recovered: 201.94 m (102.98%)  
**Lithology:**  
Unit I: clayey nannofossil ooze

**Principal results:** Site 1083 is the deep-water drill site (2180 m) of the Walvis Ridge/Walvis Basin transect, which includes Ocean Drilling Program Sites 1081 and 1082 and Deep Sea Drilling Project Sites 532 and 362. Because of its relatively low sedimentation rates, one of the main objectives for drilling at Site 1083 is to provide an extended advanced hydraulic piston core (APC) record back in time. The greater water depth should also result in well-expressed carbonate cycles via cyclic dissolu-

<sup>1</sup>Wefer, G., Berger, W.H., Richter, C., et al., 1998. *Proc. ODP, Init. Repts.*, 175: College Station, TX (Ocean Drilling Program).

<sup>2</sup>Shipboard Scientific Party is given in the list preceding the Table of Contents.

tion intensity. In addition, this site is farthest from shore and should have the best representation of pelagic signals.

Four holes were cored with the APC at Site 1083 to a maximum depth of 202.3 meters below seafloor (mbsf), which recovered a relatively continuous hemipelagic sedimentary section spanning the last 2.6 m.y. Hole 1083A was cored with the APC to 201.3 mbsf. At Hole 1083B, 22 APC cores were taken to 202.3 mbsf. One failed mudline core was taken at Hole 1083C, and Hole 1078D was cored with the APC to 196.1 mbsf.

The sediments form one lithostratigraphic unit composed of moderately bioturbated clayey nannofossil ooze. This unit has been subdivided into two subunits based on the changing abundance of diatoms, which become more abundant below 130 mbsf. The stratigraphic variation in diatom abundance and the lithostratigraphic definitions are comparable to those at Sites 1081 and 1082. A major characteristic of sediments at Site 1083 is the repeated occurrence of dark–light color cycles throughout the drilled sequence. Similar to Site 1082, the lighter colored cycles are more calcium carbonate–rich compared with the adjacent, more clay-rich, darker colored cycles. Clay-rich intervals are generally 60 to 150 cm thick and occur approximately every 2 to 5 m.

The detrital component of the sediments consists of clay with rare silt-sized, angular and subangular, mono- and polycrystalline quartz and feldspar grains. Muscovite and biotite are present in trace amounts. Grain sizes of identifiable detrital components are relatively constant. Authigenic minerals, such as framboidal pyrite and dolomite rhombs, are rare or present in trace abundances only. Carbonate minerals are generally rare to frequent in abundance and, at times, are common.

The biogenic fraction of the sediment revealed abundant to very abundant nannofossils, abundant to common foraminifer fragments, rare siliceous sponge spicules, and trace amounts of radiolarians and silico-flagellates. Diatom abundances vary from common to barren. The relative abundances of the biogenic components change frequently within one core. The intercalated dark olive-brown and black clay intervals have distinctly lower abundances of biogenic components and occasionally show higher abundances of silt-sized mono- and polycrystalline quartz grains.

Sedimentation rates range from 60 to 140 m/m.y., with the highest values located within the last 0.26 m.y. and between 0.8 and 0.96 Ma (from the onset of the Jaramillo Chron to the onset of the Brunhes Chron).

An integrated biostratigraphic framework composed of both calcareous and siliceous microfossils was established, resulting in a well-constrained age model for Site 1083. Preservation of nannofossil specimens is good to very good. The scarcity of the late Pliocene index species *Discoaster* is probably related to colder than average surface-water temperatures (a combination of increased upwelling intensity and advection of subantarctic surface water) over the southwest African and Namibian continental margins during the last 500 k.y. of the Neogene. The changes in planktonic foraminiferal species indicate a northward shift in position of the Benguela Current associated with a shift in Southern Ocean circulation, or a reduced seasonality in southerly penetration of the Angola Current. Alternatively, the biotic change may indicate increased advection of Southern Ocean water in the Benguela Current system, or a combination of all factors. Radiolarians are present throughout. In most of the investigated samples, radiolarians are abundant and preservation is good. Diatom preservation is moderate. As was the case for Sites 1081 and 1082, the record of diatom abundance points to high deposition rates during the late Pliocene and early Pleistocene. The diatom assemblage is similar to that at Sites 1081 and 1082 and consists mainly of a mixture of upwelling-indicator and oceanic species. Two middle- to high-latitude cold-water indicator species suggest periods of intensified Southern Ocean input into the Benguela Current system.

A complete magnetostratigraphy was generated at Site 1083 after alternating-field (AF) demagnetization at 20 mT. All chrons from the Brunhes (C1n) to the termination of the Gauss (C2An) at 2.58 Ma could be identified.

Dark–light color cycles, in which concentrations of calcium carbonate and organic carbon ( $C_{org}$ ) vary between 17 and 82 wt% and between 0.7 and 7.5 wt%, respectively, reflect fluctuations in the elevated marine pro-

duction associated with the Benguela Current. Most interstitial water chemical trends are intermediate between the neighboring Walvis Sites 1081 and 1082. Sulfate is completely consumed within the upper 25 mbsf; both alkalinity and ammonium display strong increases through this depth range. The concentration of interstitial water strontium reaches a maximum that is two to three times higher than that observed at Sites 1081 and 1082, reflecting the greater availability of biogenic calcite at Site 1083.

Physical sediment properties were determined both by high-resolution multisensor track (MST) core logging and index properties measurements. Magnetic susceptibility and gamma-ray attenuation porosity evaluator (GRAPE) signals reveal pronounced cyclicities, which were used for high-quality stratigraphic correlation in conjunction with digital color data.

Of the Walvis Ridge/Walvis Bay transect sites, 1083 stands out because of its excellent microfossil record, which comprises both calcareous (foraminifers and nannofossils) and siliceous fossils (diatoms and radiolarians). This will allow the intercalibration of the messages contained in these various assemblages regarding the history of change in current regimes and upwelling. With the results obtained from this and other sites in this transect, a very exact reconstruction of conditions should be possible for the last 2.6 m.y. Intercalibration of physical properties (MST data and sediment color) and of chemical stratigraphy ( $CaCO_3$  and  $C_{org}$ ) with well-constrained information from microfossils should be of special interest at this site.

## BACKGROUND AND OBJECTIVES

For a discussion of the background and objectives for Site 1083 see “Background and Objectives” section, “Site 1082” chapter (this volume).

## OPERATIONS

### Hole 1083A (Proposed Site WB-C)

The 55-nmi voyage to Site 1083 was accomplished at an average speed of 12.5 kt. The vessel approached the Global Positioning System coordinates of the site, and a beacon was deployed at 0510 hr on 17 September. Hole 1083A was spudded with the APC at 1000 hr. The seafloor depth was established from the recovery of the first core at 2178.1 meters below sea level (mbsl). APC coring advanced without incident to 201.3 mbsf (Table 1; also see the expanded core summary table on CD-ROM, back pocket, this volume), with 92.1% recovery. APC refusal was reached when the core barrel of Core 175-1083A-22H got stuck and required redrilling. Cores were oriented starting with Core 175-1083A-3H. The bit cleared the seafloor at 0225 hr on 18 September, thereby ending operations at Hole 1083A.

### Hole 1083B

The vessel was offset 30 m to the south, and Hole 1083B was spudded with the APC at 0405 hr. The recovery of the first core established the seafloor depth at 2183.1 mbsl (Table 1). APC coring advanced to 202.3 mbsf, with 102.0% recovery. The last core (175-1083B-22H) required redrilling to free the stuck core barrel. Cores were oriented starting with Core 175-1083A-4H. The bit cleared the seafloor at 2110 hr on 18 September.

### Holes 1083C and 1083D

The vessel was offset 30 m to the south. Hole 1083C consists of one failed mudline core. Hole 1083D was spudded with the APC at 2350 hr on 18 September. The recovery of the first core established the seafloor depth at 2178.3 mbsl. APC coring advanced to 196.1 mbsf, with 103.0% recovery (Table 1). Cores were oriented starting

**Table 1. Coring summary for Site 1083.**

Core	Date (Sept 1997)	Time (UTC)	Interval (mbsf)	Length cored (m)	Length recovered (m)	Recovery (%)
<b>175-1083A-</b>						
1H	17	1010	0.0-1.8	1.8	1.79	99.4
2H	17	1050	1.8-11.3	9.5	7.47	78.6
3H	17	1120	11.3-20.8	9.5	9.69	102.0
4H	17	1200	20.8-30.3	9.5	0.00	0.0
5H	17	1240	30.3-39.8	9.5	9.94	104.6
6H	17	1320	39.8-49.3	9.5	2.67	28.1
7H	17	1405	49.3-58.8	9.5	9.83	103.5
8H	17	1445	58.8-68.3	9.5	9.94	104.6
9H	17	1530	68.3-77.8	9.5	9.59	100.9
10H	17	1615	77.8-87.3	9.5	9.85	103.7
11H	17	1655	87.3-96.8	9.5	9.28	97.7
12H	17	1740	96.8-106.3	9.5	9.91	104.3
13H	17	1820	106.3-115.8	9.5	8.94	94.1
14H	17	1905	115.8-125.3	9.5	8.79	92.5
15H	17	1950	125.3-134.8	9.5	9.54	100.4
16H	17	2035	134.8-144.3	9.5	9.72	102.3
17H	17	2120	144.3-153.8	9.5	9.87	103.9
18H	17	2200	153.8-163.3	9.5	8.86	93.3
19H	17	2245	163.3-172.8	9.5	9.97	104.9
20H	17	2330	172.8-182.3	9.5	9.99	105.2
21H	18	0015	182.3-191.8	9.5	9.98	105.1
22H	18	0120	191.8-201.3	9.5	9.70	102.1
Coring totals:				201.3	185.32	92.1
<b>175-1083B-</b>						
1H	18	0420	0.0-2.8	2.8	2.85	101.8
2H	18	0455	2.8-12.3	9.5	8.78	92.4
3H	18	0535	12.3-21.8	9.5	9.81	103.3
4H	18	0615	21.8-31.3	9.5	9.60	101.1
5H	18	0710	31.3-40.8	9.5	6.33	66.6
6H	18	0745	40.8-50.3	9.5	10.12	106.5
7H	18	0825	50.3-59.8	9.5	10.10	106.3
8H	18	0900	59.8-69.3	9.5	9.83	103.5
9H	18	0935	69.3-78.8	9.5	8.82	92.8
10H	18	1010	78.8-88.3	9.5	10.11	106.4
11H	18	1045	88.3-97.8	9.5	10.02	105.5
12H	18	1125	97.8-107.3	9.5	10.16	106.9
13H	18	1205	107.3-116.8	9.5	10.08	106.1
14H	18	1245	116.8-126.3	9.5	10.17	107.1
15H	18	1330	126.3-135.8	9.5	9.89	104.1
16H	18	1410	135.8-145.3	9.5	10.05	105.8
17H	18	1455	145.3-154.8	9.5	9.83	103.5
18H	18	1700	154.8-164.3	9.5	9.82	103.4
19H	18	1810	164.3-173.8	9.5	9.96	104.8
20H	18	1855	173.8-183.3	9.5	10.03	105.6
21H	18	1940	183.3-192.8	9.5	10.10	106.3
22H	18	2050	192.8-202.3	9.5	9.95	104.7
Coring totals:				202.3	206.41	102.0
<b>175-1083C-</b>						
1H	18	2320	0-9.5	9.5	9.78	102.9
Coring totals:				9.5	9.78	102.9
<b>175-1083D-</b>						
1H	19	0005	0.0-6.1	6.1	6.16	101.0
2H	19	0040	6.1-15.6	9.5	9.27	97.6
3H	19	0120	15.6-25.1	9.5	9.89	104.1
4H	19	0200	25.1-34.6	9.5	9.55	100.5
5H	19	0235	34.6-44.1	9.5	8.99	94.6
6H	19	0315	44.1-53.6	9.5	9.83	103.5
7H	19	0350	53.6-63.1	9.5	9.92	104.4
8H	19	0430	63.1-72.6	9.5	9.93	104.5
9H	19	0510	72.6-82.1	9.5	9.29	97.8
10H	19	0550	82.1-91.6	9.5	9.89	104.1
11H	19	0630	91.6-101.1	9.5	9.89	104.1
12H	19	0705	101.1-110.6	9.5	10.02	105.5
13H	19	0745	110.6-120.1	9.5	9.82	103.4
14H	19	0825	120.1-129.6	9.5	10.10	106.3
15H	19	0905	129.6-139.1	9.5	9.91	104.3
16H	19	0945	139.1-148.6	9.5	9.49	99.9
17H	19	1030	148.6-158.1	9.5	9.91	104.3
18H	19	1110	158.1-167.6	9.5	10.10	106.3
19H	19	1140	167.6-177.1	9.5	9.98	105.1
20H	19	1230	177.1-186.6	9.5	10.11	106.4
21H	19	1315	186.6-196.1	9.5	9.89	104.1
Coring totals:				196.1	201.94	103.0

Notes: UTC = Universal Time Coordinated. An expanded version of this coring summary table that includes lengths and depths of sections and comments on sampling is included on CD-ROM (back pocket, this volume).

with Core 175-1083A-3H. The drill string was retrieved, with the bit clearing the seafloor at 1420 hr and the plane of the rotary table at 1855 hr on 19 September. The beacon was recovered, and the hydrophones and thrusters were retracted. The vessel was under way to Site 1084 at 1900 hr on 19 September.

## SITE GEOPHYSICS

For a discussion of site geophysics at Site 1083, see "Site Geophysics" section, "Site 1081" chapter (this volume).

## LITHOSTRATIGRAPHY

### Description of Lithostratigraphic Unit

#### Unit I

Intervals: 175-1083A-1H-1, 0 cm through 175-1083A-22H-7; 175-1083B-1H-1, 0 cm, through 175-1083B-22H-7; 175-1083C-1H-1, 0 cm, to 1H-7, 55 cm; 175-1083D-1H-1, 0 cm, through 175-1083D-21H-7

Age: Holocene to late Pliocene

Depth: 175-1083A: 0–201 mbsf; 175-1083B: 0–202 mbsf; 175-1083C: 0–9 mbsf; 175-1083D: 0–196 mbsf

Four holes were drilled at Site 1083 with a maximum penetration of 202.75 mbsf (see Fig. 1). Sediments from Site 1083 form one lithostratigraphic unit composed of moderately bioturbated clayey nannofossil ooze. This unit has been subdivided into two Subunits, IA and IB, based on the changing abundance of diatoms. Subunit IA extends to Core 15 at Holes 1083A, 1083B, and 1083D and with the exception of few 1- to 1.5-m-thick diatom-rich intervals, contains diatoms in rare to frequent abundance. In Subunit IB, diatoms become consistently common. The stratigraphic variation in diatom abundance and the definition of the subunits is comparable to those at Sites 1081 and 1082 (see "Lithostratigraphy" sections, "Site 1081" and "Site 1082" chapters, this volume). A major characteristic of sediments from Site 1083 is the repeated occurrence of dark–light color cycles throughout the drilled sedimentary succession. As at Site 1082, the lighter colored cycles are more calcium carbonate–rich compared to the adjacent more clay-rich, darker colored cycles. Clay-rich intervals are generally 60 to 150 cm thick and occur approximately every 2 to 5 m.

#### Subunit IA

Intervals: 175-1083A-1H-1, 0 cm, through 175-1083A-15H-6; 175-1083B-1H-1, 0 cm, through 175-1083B-15H-3; 175-1083D-1H-1, 0 cm, through 175-1083D-15H-4

Age: Holocene to Pleistocene

Depth: 175-1083A: 0–133 mbsf; 175-1083B: 0–131 mbsf; 175-1083D: 0–136 mbsf

Subunit IA is composed of moderately bioturbated intervals of pale yellow (5Y 7/3) and pale olive (5Y 6/3) foraminifer-rich clayey nannofossil ooze. Dark layers of olive-gray (5Y 3/2 to 5Y 4/2) and olive (5Y 4/3) diatom-bearing or diatom-rich nannofossil clay are present throughout this subunit. Similar to Site 1082 (see "Lithostratigraphy" section, "Site 1082" chapter, this volume), sediments in Subunit IA have high carbonate and organic carbon contents, which average 68 and 2.3 wt%, respectively (see "Organic Geochemistry" section, this chapter). The contact between Subunits IA and IB is relatively sharp and occurs below a dark nannofossil clay layer in Cores 175-1083A-15H-6, 175-1083B-15H-3, and 175-1083D-15H-4. The boundary is marked by an increase in diatom abundance from diatom-bearing and sporadically diatom-rich to consistently diatom-rich.

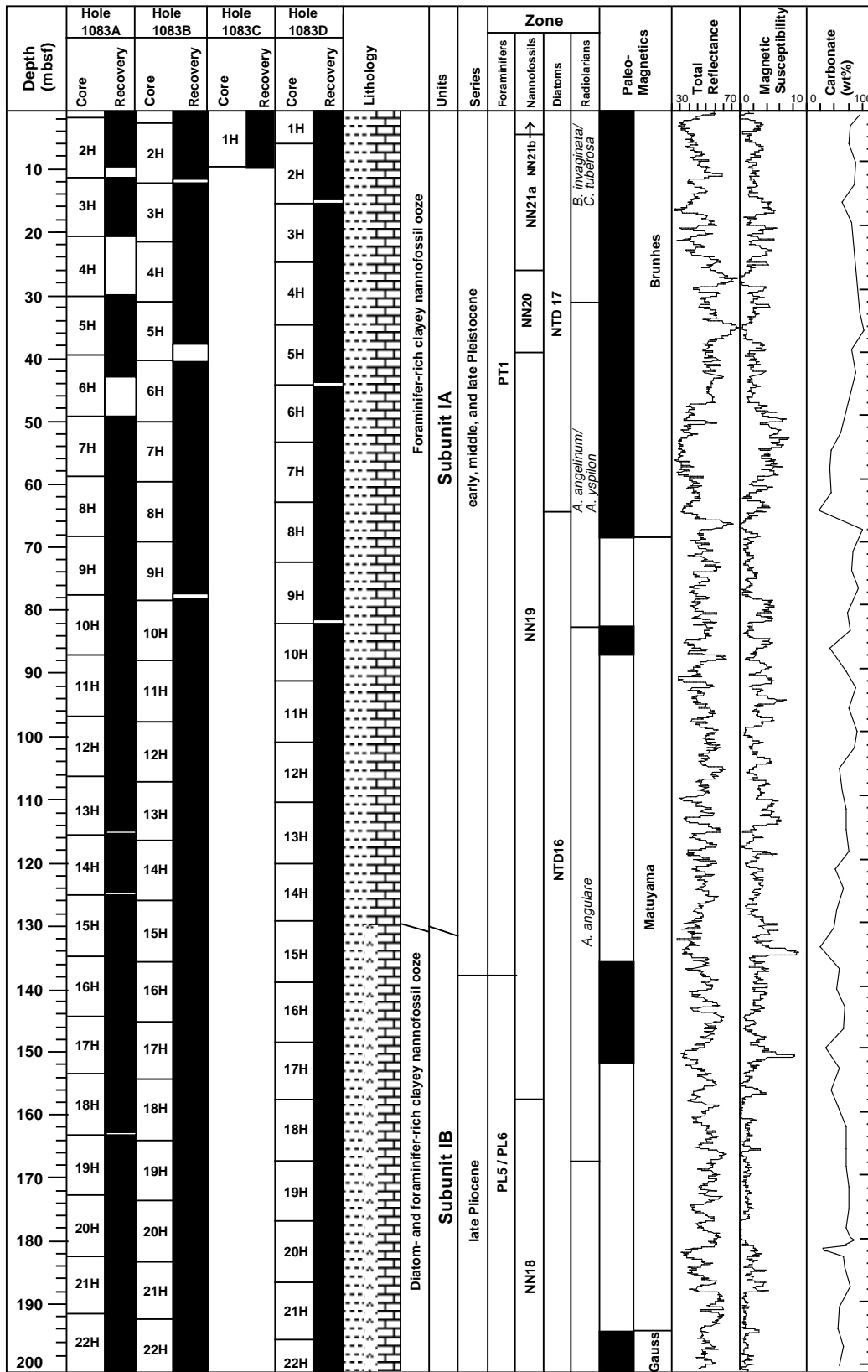


Figure 1. Composite stratigraphic section for Site 1083 showing core recovery in all holes, a simplified summary of lithology, age, total reflectance (400–700 nm), magnetic susceptibility, and calcium carbonate content.

### Subunit IB

Intervals: 175-1083A-15H-6 through 175-1083A-22H-7; 175-1083B-15H-3 through 175-1083B-22H-7; 175-1083D-15H-4 through 175-1083D-21H-7

Age: late Pliocene

Depth: 175-1083A: 133–201.2 mbsf; 175-1083B: 131–202.8 mbsf; 175-1083D: 136–196.1 mbsf

Subunit IB is composed of intervals of pale yellow (5Y 7/4), pale olive (5Y 6/3) diatom- and foraminifer-rich clayey nannofossil ooze. Olive (5Y 4/3), and olive-gray (5Y 4/2) nannofossil-rich clay and nannofossil clay are present as 30- to 100-cm-thick intervals and are characterized by lower abundances of diatoms and foraminifers. Compared to Subunit IA, abundances of diatoms in the nannofossil ooze are relatively constant. Concentrations of calcium carbonate and organic carbon average 48 and 2.8 wt.%, respectively, which is slightly lower than their average concentrations in Subunit IA.

### Synthesis of Smear-Slide Analyses

Smear-slide analyses indicate that the detrital component of the sediments in the two subunits consists of clay with rare silt-sized, angular and subangular, mono- and polycrystalline quartz, and feldspar grains. Muscovite and biotite are present in trace amounts. Grain sizes of identifiable detrital components are relatively constant throughout the two lithostratigraphic subunits. Authigenic minerals, such as framboidal pyrite and dolomite rhombs, are rare or present in trace amounts only. Carbonate minerals are generally rare to frequent in abundance. Carbonate minerals are common in the smear slides taken at Sections 175-1083A-15H-2, 50 cm, and 22H-6, 80 cm, and are associated with nannofossil ooze.

Smear-slide analyses of sediment from Subunit IA reveal abundant to very abundant nannofossils, abundant to common foraminifer fragments, rare siliceous sponge spicules, and trace amounts of radiolarians and silicoflagellates. Diatom abundances vary from common to barren. The relative abundance of the biogenic components changes frequently within any given core. Individual intervals are between 30 and 250 cm thick. The intercalated dark olive-brown and black clay intervals have distinctly lower abundances of biogenic components and occasionally show higher abundances of silt-sized mono- and polycrystalline quartz grains. Smear slides from the darkest layers contain common amorphous brown aggregates of organic matter. In Subunit IA, dark layers have consistently higher abundances of diatoms compared with the adjacent lighter colored intervals. In Subunit IB, abundances of diatoms are lower within the dark layers than within the adjacent lighter colored intervals. Furthermore, nannofossils and foraminifer fragments are, in general, less abundant in Subunit IA than in Subunit IB. These relationships suggest varying dilution of the biogenic component by clastic detritus and possible coupling among diatom productivity, abundance of organic matter, and the dissolution of calcareous microfossils.

### Spectrophotometry

Color data were measured every 4 cm for Holes 1083A, 1083B, and 1083D. At Site 1083, total reflectance values range between 30% and 65% (Fig. 2). Total reflectance records for the three holes are very similar, except for the upper 50 mbsf of Hole 1083A where core recovery was poor. Variations in total reflectance generally reflect the relative proportions of calcium carbonate to clay. There is a similarity between the top 70 mbsf at Site 1083 and the top 100 mbsf at Site 1082 (see "Litho-stratigraphy" section, "Site 1082" chapter, this volume) in the total reflectance data. Using the age model (see "Biostratigraphy and Sedimentation Rates" and "Paleomagnetism" sections, this chapter), high total reflectance values between 25 and 50

mbsf at Hole 1083D correspond to marine oxygen-isotope Stages 9 and 11; this is also observed at Site 1082 (see "Lithostratigraphy" section, "Site 1082" chapter, this volume). Marine oxygen-isotope Stage 19 can also be identified from the peak in the total reflectance values at 68 mbsf (Holes 1083A, 1083B, and 1083D) and is supported by the identification of the Brunhes/Matuyama magnetic reversal at this stratigraphic position (see "Paleomagnetism" section, this chapter). The total reflectance between 150 and 200 mbsf at all three holes exhibits a pronounced cyclicality (see Fig. 2). The age of this interval is constrained by the identification of the Olduvai (1.99 Ma) and Gauss (2.6 Ma) magnetic reversals (see "Paleomagnetism" section, this chapter) and suggests that the cyclicality in the total reflectance record is on the order of 40 k.y. These preliminary results suggest that total reflectance may be used as a high-resolution stratigraphic tool to reconstruct glacial/interglacial cycles.

### BIOSTRATIGRAPHY AND SEDIMENTATION RATES

The sediment recovered from Site 1083 represents a relatively continuous hemipelagic section spanning the last 2.6 m.y. The micro-paleontological studies were carried out on core-catcher samples from Hole 1083A. Additional samples from within the cores were examined to improve the biostratigraphic resolution. An integrated biostratigraphic framework composed of both calcareous and siliceous microfossils was established (Fig. 3), resulting in a well-constrained age model for Site 1083. Sedimentation rates range from 6 to 14 cm/k.y. with highest values located within the last 260 k.y., as well as be-

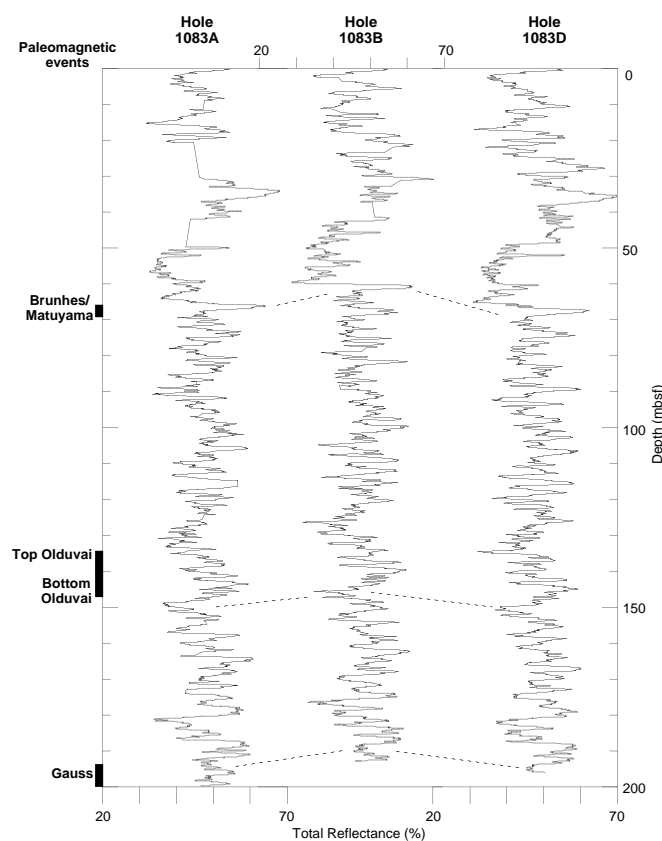


Figure 2. Stratigraphic variation in the total reflectance at Holes 1083A, 1083B, and 1083D.

tween 0.8 and 0.96 Ma (from the onset of the Jaramillo Chron to the onset of the Brunhes Chron).

### Calcareous Nannofossils

In addition to Hole 1083A, the top part of Hole 1083B was studied to constrain the 0.26-Ma datum event (last occurrence [LO] of the *Gephyrocapsa caribbeanica* acme). This biohorizon could not be precisely located at Hole 1083A because of the poor recovery of some of the upper cores. Preservation of nannofossil specimens is good to very good. Calcareous nannofossils are abundant to very abundant throughout the entire section. Reworked specimens (essentially Pliocene) are common in Sample 175-1083A-7H-CC, then rare to common within every investigated sample from the lower half of Site 1083 (Cores 175-1083A-10H through 22H).

Site 1083 terminated within the upper Pliocene sediment. The scarcity of *Discoaster* index species in assemblages from the bottom part of Hole 1083A prevents us from assigning a zone to the deeper samples. Paleomagnetic data (see "Paleomagnetism" section, this

chapter) suggest that Core 175-1083A-22H terminated near the NN17/NN16 zonal transition (~2.6 Ma). Ten nannofossil biohorizons, including five zonal boundary events, were recognized at Hole 1083A (Table 2; Fig. 3). Most datum events could be constrained within a range of ±4 m.

### Zone NN21b

This zone only covers the top 3 mbsf of Hole 1083A. The Zone NN21b/NN21a boundary (0.09 Ma) is found between Samples 175-1083A-1H-CC and 2H-2, 90 cm.

### Zone NN21a

Sedimentation rates estimates within this 170-k.y. interval should be used with caution. The base of Zone NN21a at Hole 1083A is located within an unrecovered sedimentary sequence (Core 175-1083A-4H). This datum event (LO of the *Gephyrocapsa caribbean-*

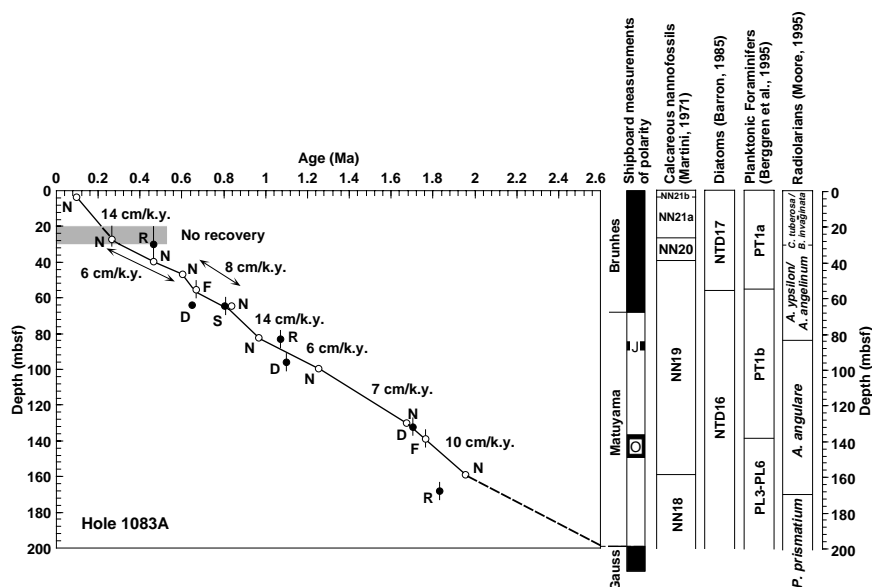


Figure 3. Age-depth plot and sedimentation rates estimated from calcareous microfossil (open circles; F = planktonic foraminifers and N = calcareous nannofossils) and siliceous microfossil (solid circles; D = diatoms, R = radiolarians, and S = silicoflagellates) datums at Hole 1083A. Gray shading = no recovery.

Table 2. Microfossil datums at Holes 1083A and 1083B.

Fossil group	Event	Age (Ma)	Zone (base)		Core, section, interval (cm)		Depth (mbsf)		
			A	B	Top	Bottom	Top	Bottom	Mean
N	FO <i>Emiliania huxleyi</i> acme	0.09	NN21b		175-1083A-1H-CC	175-1083A-2H-2, 90	1.74	4.20	2.97
N	FO <i>Emiliania huxleyi</i>	0.26	NN21a	CN15	3H-CC	5H-1, 140	20.94	31.70	26.32
N	LO <i>Gephyrocapsa caribbeanica</i> acme	0.26	NN21a	CN15	3H-CC	5H-1, 140	20.94	31.70	26.32
N	LO <i>Pseudoemiliania lacunosa</i>	0.46	NN20	CN14b	5H-6, 10	5H-CC	37.80	40.19	39.00
R	LO <i>Axoprumum angelinum</i>	0.46			3H-CC	5H-CC	20.94	40.19	30.57
N	LO Small <i>Gephyrocapsa</i> acme (Weaver, 1993)	0.60			6H-CC	7H-1, 80	42.42	50.10	46.26
D	LO <i>Nitzschia reinholdii</i>	0.69			7H-CC	8H-CC	59.08	68.89	63.89
S	LO <i>Bachmannocena quadrangula</i>	0.80			7H-CC	8H-CC	59.08	68.89	63.89
N	LO <i>Reticulofenestra asanoi</i>	0.83			8H-3, 40	8H-5, 60	62.20	65.30	63.75
N	LO Small <i>Gephyrocapsa</i> acme (Gartner, 1977)	0.96			10H-2, 130	10H-4, 80	80.60	83.00	81.80
R	LO <i>Lamprocyrtis neoheteroporus</i>	1.07			9H-CC	10H-CC	77.84	87.60	82.72
D	LO <i>Rhizosolenia matuyama</i>	1.10			10H-CC	11H-CC	87.60	96.53	92.07
N	LO <i>Helicosphaera sellii</i>	1.25			11H-CC	12H-3, 120	96.53	101.00	98.77
N	LO <i>Calcidiscus macintyrei</i>	1.67			18H-CC	15H-CC	124.54	134.79	129.67
D	LO <i>Proboscia barboi</i>	1.68			14H-CC	15H-CC	124.54	134.79	129.67
R	LO <i>Cycladophora pliocenica</i>	1.83			18H-CC	19H-CC	162.61	173.22	129.67
N	LO <i>Discoaster brouweri</i>	1.95	NN19	CN13a	17H-CC	18H-CC	154.12	162.91	158.52
N	FO <i>Emiliania huxleyi</i>	0.26	NN21a	CN15	175-1083B-3H-3, 130	175-1083B-3H-5, 130	16.60	19.60	18.10
N	LO <i>Gephyrocapsa caribbeanica</i> acme	0.26	NN21a	CN15	3H-3, 130	3H-5, 130	16.60	19.60	18.10

Notes: Fossil group: N = calcareous nannofossils; R = radiolarians; D = diatoms; and S = silicoflagellates. FO = first occurrence and LO = last occurrence. Zonal codes refer to the standard calcareous nannofossil zonations of (A) Martini (1971) and (B) Okada and Bukry (1980).

ica acme) was, however, recognized at Hole 1083B between Samples 175-1083B-3H-3, 130 cm, and 3H-5, 130 cm.

### Zone NN20

As documented in the more northern Leg 175 sites, this 0.2-m.y. interval is constrained within a narrow depth range (~13 m). The Zone NN20/NN19 boundary is identified within the lower part of Core 175-1083A-5H at a mean depth of 39 mbsf.

### Zone NN19

Most of the sedimentary sequence recovered from Site 1083 belongs to this stratigraphic interval (0.46–1.95 Ma). The stratigraphic resolution of the upper half of Zone NN19 is particularly well constrained, with five nannofossil biohorizons recognized between ~40 and 80 mbsf. Reworking of late and early Pliocene specimens is common throughout the lower half of this stratigraphic unit.

### Zone NN18

The Zone NN19/NN18 boundary event (LO of *Discoaster brouweri*) is recognized between Samples 175-1083A-17H-CC and 18H-CC. As discussed earlier, Site 1083 probably terminated near or passed the NN17/NN16 zonal boundary. Among the four *Discoaster* species commonly present in calcareous nannofossil assemblages representative of Zone NN17, *D. brouweri*, which extends from Zones NN10 to NN18, was the only species recognized in Samples 18H-CC through 22H-CC. This scarcity in late Pliocene index species is probably related to colder than average surface-water temperature (a combination of increased upwelling intensity and advection of subantarctic surface water) over the southwest African and Namibian continental margins during the last 500 k.y. of the Neogene (see “Diatoms” and “Planktonic Foraminifers” sections, this chapter).

## Planktonic Foraminifers

The uppermost assemblage (Sample 175-1083A-1H-CC) is dominated by *Globigerina bulloides*, and *Globorotalia inflata* is abundant (Table 3). This pattern is maintained downcore. The remainder of the uppermost assemblage includes *Orbulina universa*, *Neogloboquadrina pachyderma* (dextral and sinistral), *Hastigerina siphonifera*, *Globorotalia truncatulinoides*, *Globorotalia scitula*, *Globorotalia crassaformis*, *Globigerinoides sacculifer*, *Globigerinoides ruber*, *Globigerina falconensis*, *Globigerina umbilicata*, and *Beella digitata*, and is consistent with the position within the Benguela Current.

Core 175-1083A-5H was sampled to identify faunas representative of possible glacial (green clay)/interglacial (white carbonate ooze) changes (see “Lithostratigraphy” section, this chapter, for a complete description of the sediments). The assemblages within the green clay (Sample 5H-1, 74–76 cm) are similar to the assemblage described above: they are dominated by *Globigerina bulloides* and *G. inflata* and also include *G. umbilicata*, *O. universa*, *N. pachyderma* (sinistral and dextral), *G. crassaformis*, and *G. truncatulinoides*. The assemblage within the white mud (Sample 5H-3, 64–66 cm) is dominated by warm-water faunas, such as *G. ruber*, *N. dutertrei*, *O. universa*, and *G. menardii*, and indicates the influence of the warm-water Angola Current in the region.

The presence of *G. menardii* and *G. dutertrei* is used to trace a strong Angola Current contribution downcore (Fig. 4A). Samples 175-1083A-3H-CC, 11H-CC, and 15H-CC contain both *Globorotalia menardii* and *N. dutertrei*. *G. menardii* is present in Samples 175-1083A-2H-CC and 8H-CC, but *N. dutertrei* is not. These species are absent in Samples 175-1083A-5H-CC through 7H-CC and 17H-CC through 22H-CC, which is coincident with an influx of subantarctic diatom species (Fig. 4A). The change in fauna and flora would seem to indicate a northward shift in position of the Benguela Current. It is

**Table 3. Relative abundance, presence or absence, and overall abundance of planktonic foraminifers at Hole 1083A.**

Core, section, interval	Depth (mbsf)	Overall abundance	Dissolution	<i>Globigerinoides ruber</i>	<i>Globigerina bulloides</i>	<i>Globorotalia inflata</i>	<i>Neogloboquadrina dutertrei</i>	<i>Neogloboquadrina pachyderma</i> (dextral)	<i>Neogloboquadrina pachyderma</i> (sinistral)	<i>Globorotalia crassaformis</i>	<i>Globorotalia truncatulinoides</i>	<i>Globorotalia tosaensis</i>	<i>Globorotalia menardii</i>	<i>Neogloboquadrina dutertrei</i>
175-1083A-1H-CC	1.7	5		D	A					P				
2H-CC	9.2	5		A	D					P			P	
3H-CC	20.9	5		D	D					P			P	P
5H-CC	40.2	4	4	D	A					P				
6H-CC	42.4	5	4	A	D				A	P				
7H-CC	59.1	4	2		D									
8H-CC	68.7	5	5		D	D				P	P	P		
9H-CC	77.8				A		D			P	P		P	
11H-CC	96.5	5	5	D	D	A	A			P	P	P	P	
13H-CC	115.2	5	5	D	D	A				P	P		P	
15H-CC	134.8	5	5		D	A	D			P		P	P	
16H-CC	144.5	4	4		D				D					P
17H-CC	154.1				D	D								
18H-CC	162.6	4	4		D									
19H-CC	173.2	2	2		D	D								
22H-CC	201.5	4	4		D									

Notes: D = dominant (>30%) and A = abundant (10%–30%) components of the assemblage are shown. Presence (P) and absence (A) are also shown for select species. Overall abundance is classified as 0 = barren; 1 = trace; 2 = rare; 3 = few; 4 = common; and 5 = abundant. Dissolution is grouped as 2 = some dissolution; 4 = moderate dissolution; and 5 = no dissolution.

unlikely that the absence of these species is caused by dissolution, because *G. menardii* is quite resistant to dissolution.

The planktonic foraminifers are generally abundant and better preserved than at previous sites (Fig. 4B). The last-appearance datum of *G. tosaensis* defines the top of Zone Pt1a and constrains the age to the middle Pleistocene (LO = 0.65 Ma). The species last occurs in Sample 175-1083A-8H-CC (68.7 mbsf), but its absence in Sample 7H-CC may be the result of dissolution in that interval. The 0.65-Ma first-appearance datum (FAD) is therefore placed at (55 mbsf), between Samples 8H-CC and 6H-CC (42.4 mbsf), and is in agreement with datums from the other microfossil groups. The Pliocene/Pleistocene boundary (1.77 Ma) and the base of Zone Pt1a are marked by the FAD of *G. truncatulinoides*. It is present in Sample 175-1083A-15H-CC (134.8 mbsf), absent in Sample 16H-CC (144.5 mbsf), and placed at 139 mbsf. The species *G. crassaformis viola* (late Pliocene to early Pleistocene) is present in Samples 175-1083A-9H-CC through 18H-CC. The LO of *G. crassaformis viola* in Sample 9H-CC suggests an early Pleistocene age and is in agreement with the identification of the Brunhes/Matuyama boundary (early/middle Pleistocene) in the base of Core 8H. *G. crassaformis viola* is not present in Samples 175-1083A-19H-CC through 22H-CC, and its absence indicates an age equal to or older than the early late Pliocene Zone PL5. A position with Zone PL5 is in agreement with paleomagnetic analyses (see “Paleomagnetism” section, this chapter), which place the Matuyama/Gauss boundary (within Zone PL5) within Core 22X. The presence of *G. pseudomiocenica* in Sample 22H-CC confirms a Pliocene age for that sample.

## Benthic Foraminifers

The abundance of benthic foraminifers at Hole 1083A is high in the upper part of the investigated interval, but decreases downcore to few to rare.

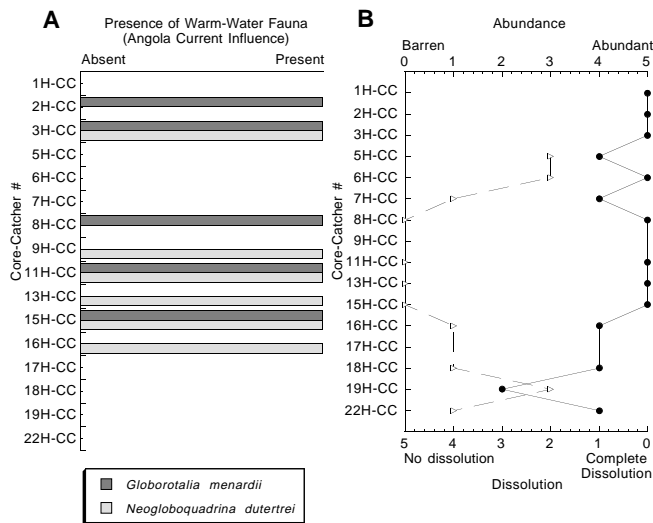


Figure 4. **A.** Presence/absence of *G. menardii* (shaded) and *N. dutertrei* (hatched). The presence of warm-water fauna indicates a strong Angola Current influence. The absence of the species correlates with an influx of subantarctic diatom species. **B.** Dissolution (dashed line with triangles) and abundance (solid line with circles). Abundance is classified as 0 = barren; 1 = trace; 2 = rare; 3 = few; 4 = common; and 5 = abundant. Dissolution is grouped as 2 = some dissolution; 4 = moderate dissolution; and 5 = no dissolution.

The dominating benthic foraminiferal species in the uppermost core catchers (Sample 175-1083A-1H-CC; 1.74 mbsf) are *Bulimina aculeata* and *Cassidulina laevigata* (Table 4). The interval, comprising core-catchers 175-1083A-2H-CC through 9H-CC (9.22–77.84 mbsf), is dominated by *Bulimina exilis* and *Cassidulina laevigata* (Table 4). Other important species in this interval are *Fursenkoina* sp. 1 and *Oridorsalis umbonatus*. The lowermost interval, from core-catcher 175-1083A-11H-CC to the bottom of the hole (96.53–192.13 mbsf), is dominated by *Cibicidoides wuellerstorfi*, *Melonis barleeanum*, *Uvigerina hispidocostata*, and *Uvigerina peregrina* (Table 4).

### Radiolarians

Radiolarians are present in all of the core-catcher samples from Hole 1083A (Table 5). In most of the investigated samples, radiolarians are abundant, and preservation is good. The radiolarian fauna indicates a Quaternary to late Pliocene age for Hole 1083A. No apparent reworking has been identified.

The absence of *Axoprunum angelinum* indicates that the uppermost cores (Samples 175-1083A-1H-CC, 2H-CC, and 3H-CC) are within either the Pleistocene *Collosphaera tuberosa* Zone or the Pleistocene to Holocene *Buccinosphaera invaginata* Zone of Moore (1995). A finer zonal resolution could not be achieved because of the absence of *B. invaginata*.

Although the diagnostic species *Anthocyrtidium angulare* is absent throughout the core, Samples 175-1083A-5H-CC through 9H-CC are approximately assigned to the Pleistocene *A. angelinum* Zone or *Amphirhopalum ypsilon* Zone of Moore (1995) based on the presence of *A. angelinum* and the absence of *Lamprocyrtis neoheteroporos*. The diagnostic species *C. tuberosa* (which is used to recognize the *A. angelinum* and *A. ypsilon* Zones) is absent throughout the core.

Although the diagnostic species *Anthocyrtidium angulare* and *P. prismatium* are absent throughout the core, Samples 175-1083A-10H-CC through 18H-CC are assigned to the Pleistocene *A. angulare* Zone of Moore (1995) based on the presence of *Lamprocyrtis neohet-*

*eroporos* and the absence of *Cycladophora pliocenica*, which became extinct at 1.78 Ma in the Antarctic Ocean (Caulet, 1991).

The LO of *C. pliocenica* is placed in Sample 175-1083A-19H-CC, approximating the Pliocene/Pleistocene boundary between Samples 18H-CC and 19H-CC. The presence of *Cycladophora davisiana* indicates that the deepest sample (22H-CC) is younger than 2.7 Ma, and that the lowest four samples (19H-CC through 22H-CC) are within the *P. prismatium* Zone of Moore (1995).

### Diatoms

Diatom counts and identification were carried out on smear slides and on acid-treated, sieved (20  $\mu$ m) material from core-catcher samples from Hole 1083A (Table 6). Diatom preservation is moderate throughout Hole 1083A. The record of diatom abundance points to high deposition during the late Pliocene and early Pleistocene (from ~96 mbsf to the end of the hole; see Table 6).

Samples 175-1083A-1H-CC through 7H-CC are assigned to the *Fragilariopsis* (= *Pseudoemotia*) *doliolus* Zone NTD17 based on the occurrence of *F. doliolus* stratigraphically above the LO of *Nitzschia reinholdii* in Sample 175-1083A-8H-CC. The interval from Sample 8H-CC to the end of the hole is assigned to the *Nitzschia reinholdii* Zone NTD16. As has been the case at Sites 1081 and 1082, we recorded two middle- to high-latitude cold-water indicator species, *Proboscia* (= *Simonseniella*) *curvirostris* in Sample 8H-CC (at approximately the Brunhes/Matuyama boundary) and *P. barboi* in Samples 175-1083A-15H-CC through 22H-CC (Table 6). The occurrence of these species may indicate periods of intensified subantarctic input into the Benguela Oceanic Current system (see “Nannofossils” and “Planktonic Foraminifers” sections, this chapter).

The diatom assemblage is similar to that at Sites 1081 and 1082 and consists mainly of a mixture of upwelling-indicator (*Chaetoceros* resting spores and *Thalassionema nitzschioides* var. *nitzschioides*) and oceanic species (e.g., *Azpeitia nodulifer*, *A. tabularis*, *Hemidiscus cuneiformis*, and *Thalassiothrix* spp.).

### PALEOMAGNETISM

The investigation of magnetic properties at Site 1083 included measurement of the bulk susceptibility of whole-core sections and the natural remanent magnetization (NRM) of archive-half sections and discrete samples. The Tensor tool was used to orient Cores 175-1083A-4H through 22H, Cores 175-1083B-3H through 22H, and Cores 175-1083D-3H through 21H (Table 7).

#### Natural Remanent Magnetization, Magnetic Susceptibility, and Magnetic Overprint

Measurements of NRM were made on all archive-half core sections from Holes 1083A, 1083B, and 1083D. Only one core was recovered from Hole 1083C; therefore, this hole will not be discussed further in this section. Sections from Hole 1083A were demagnetized by AF at 10 and 20 mT, and sections from Holes 1083B and 1083D were demagnetized by AF at 20 mT only. All discrete samples taken from Hole 1083A (one per section) were demagnetized by AF at 10, 20, 25, and 30 mT. Magnetic susceptibility measurements were made on whole cores from all holes as part of the MST analysis (see “Physical Properties” section, this chapter).

Magnetic susceptibility ranges between 0 and  $5 \times 10^{-5}$  (SI volume units), and the intensity of NRM after 20-mT demagnetization ranges between  $\sim 10^{-2}$  and  $\sim 10^{-4}$  A/m (Fig. 5). In general, they are inversely correlated with the total reflectance in spectrophotometry, which reflects the relative proportion of calcium carbonate to clay (see “Lithostratigraphy” section, this chapter). This correlation indicates



**Table 5. Stratigraphic distribution of radiolarians at Hole 1083A.**

Age	Zone	Core, section, interval	Depth (mbsf)	Abundance	Preservation	<i>Amphirophalum ypsilon</i>	<i>Cycladophora davisi</i>	<i>Didymocypris tetrahedralis</i>	<i>Eucypridium calvertense</i>	<i>Eucypridium teuscheri</i>	<i>Eucypridium acuminatum</i>	<i>Lamprocyclus hawaii</i>	<i>Lamprocypris nigrinae</i>	<i>Pterocanium praetextum eucolpum</i>	<i>Pterocanium trilobum</i>	<i>Spongurus pylomarticus</i>	<i>Theocorythium trachelium</i>	<i>Cycladophora cornuoides</i>	<i>Phormostichoartus corbula</i>	<i>Saturnalis circularis</i>	<i>Axoprium angelinum</i>	<i>Lamprocypris neoheteroporos</i>	<i>Phormostichoartus fistula</i>	<i>Spongaster tetras tetras</i>	<i>Lamprocypris heteroporos</i>	<i>Didymocypris avita</i>	<i>Cycladophora pliocenica</i>	<i>Cycladophora sakaii</i>	
Quaternary	<i>B. invaginata</i> – <i>C. tuberosa</i>	175-1083A-1H-CC	1.74	A	G	P	P	P	P	+	P	P	+	+	+	P	+												
Quaternary	<i>B. invaginata</i> – <i>C. tuberosa</i>	2H-CC	9.22	A	G	+	P	P	P		P	P	+	P		P	P		+	+									
Quaternary	<i>B. invaginata</i> – <i>C. tuberosa</i>	3H-CC	20.94	A	G		P	P		P	+	P		+	P		P												
Pleistocene	<i>A. angelinum</i> – <i>A. ypsilon</i>	5H-CC	40.19	A	G	+	P				P	P	+	+	P				P										
Pleistocene	<i>A. angelinum</i> – <i>A. ypsilon</i>	6H-CC	42.42	A	G		P	+	P	P	+	P	P	+	+	P	+			P									
Pleistocene	<i>A. angelinum</i> – <i>A. ypsilon</i>	7H-CC	59.08	A	G		P	P	P	P		P	P			P	+			+									
Pleistocene	<i>A. angelinum</i> – <i>A. ypsilon</i>	8H-CC	68.69	A	G		P			+	P	P	P		P	P		+		+									
Pleistocene	<i>A. angelinum</i> – <i>A. ypsilon</i>	9H-CC	77.84	A	G	+	P				P	P	+	P		P	P		+	+									
Pleistocene	<i>A. angulare</i>	10H-CC	87.60	A	G	+	P	P	P	P		P	P								P	P							
Pleistocene	<i>A. angulare</i>	11H-CC	96.53	A	G	+	P	P	P	P	+	P	P		P			+		+				+	+				
Pleistocene	<i>A. angulare</i>	12H-CC	106.66	A	G	P	P	P	P	P	+	P	P		P			+	P	+					+	+			
Pleistocene	<i>A. angulare</i>	13H-CC	115.19	A	G	P	+	P	P	P	+	P	P		P			+		+									
Pleistocene	<i>A. angulare</i>	14H-CC	124.54	A	G	+	P	P	+	+	P		P					+			P	P						P	
Pleistocene	<i>A. angulare</i>	15H-CC	134.79	A	G	+	P	P	P	P	+	P	P		P			+			P	+						P	
Pleistocene	<i>A. angulare</i>	16H-CC	144.47	A	G	P	P	P	P	P	+	P	P		P			+	+	+	P	P							
Pleistocene	<i>A. angulare</i>	17H-CC	154.12	C	G	P	+	P	P	P		P	P		P			P	P		+	P						P	
Pleistocene	<i>A. angulare</i>	18H-CC	162.61	A	G	P	P	P	P	P	+	P	P		P			P	P	P	P	P							
Pliocene	<i>P. prismatium</i>	19H-CC	173.22	A	G	P	P			P		P			P			+		P								P	
Pliocene	<i>P. prismatium</i>	20H-CC	182.72	A	G		P	+	P	P		P			P				+		P								
Pliocene	<i>P. prismatium</i>	21H-CC	192.23	C	G	P		P	+	P	P	P			P			+		+	P							P	
Pliocene	<i>P. prismatium</i>	22H-CC	201.45	A	M		P			P	+	P			P			+		P								P	

Notes: Occurrence is indicated by P = present and + = one specimen per slide. Abundance: A = abundant and C = common. Preservation: G = good and M = moderate. *B. invaginata* = *Buccinosphaera invaginata*; *C. tuberosa* = *Collosphaera tuberosa*; *A. angelinum* = *Axoprium angelinum*; *A. ypsilon* = *Amphirophalum ypsilon*; *A. angulare* = *Anthocypridium angulare*; *P. prismatium* = *Pterocanium prismatium*.

that the concentration of magnetic minerals is low in calcium carbonate-rich horizons.

We encountered a curious secondary magnetization at this site. In each core that was recovered below ~80 mbsf, inclinations deviate downcore from the expected value toward steep negative values, indicating downcore acquisition of an upward magnetic overprint. Figure 6 shows an example of Cores 175-1083B-11H through 15H, which is within the Matuyama Chron, discussed below. The inclination expected from the geocentric axial dipole model during the Matuyama Chron is 37° at this site. The inclinations near the top of each core are close to the expected value, but they change toward negative values downcore. Furthermore, cyclic inclination fluctuations are superimposed on the downcore trend, which is inversely correlated to the total reflectance from spectrophotometry (Fig. 6). This suggests a relationship between the magnetic overprint and the sediment lithology. Discrete samples, however, preserved a primary magnetization and did not show the magnetic overprint (Fig. 7). The inclinations of the discrete samples are close to those expected from the polarity (Fig. 5). This indicates that the source of the upward magnetic overprint resides in the sediments along the rim of the cores, and thus deformation of sediments along the core liner could be responsible. Sticky calcium carbonate-rich horizons may suffer more extensive deformation during coring and thus acquire a more severe magnetic overprint. However, we do not understand the deformation mechanism that produces the upward magnetization; it cannot be explained by simple drag along the core liner because the overprint has a pervasive upward direction that is independent of the core orientation (see “Paleomagnetism” section, “Site 1077” chapter, this volume). The inclinations of surface sediments above ~30 mbsf in half cores are also significantly steeper than the expected value (Fig. 5); discrete samples did not show this tendency. This phenomenon may also be related to deformation of sediments along the rim of cores.

The magnetic overprint at this site is different from the coring-induced magnetization (CIM) that is radially inward and downward in APC cores and from that of ~30° declination and downward in extended barrel (XCB) cores observed at other sites (see “Paleomagnetism” sections, “Site 1077” and “Site 1081” chapters, this volume). The downward direction of the CIM is opposite to the upward overprint here. Declinations of discrete samples (from working halves) generally agree with those of half-core (archive-half) measurements, which indicates that the radial-inward component is not significant. The upcore increase in intensity observed in the CIM, which indicates upcore growth of secondary magnetization, was not observed here. The CIM was reported from discrete samples as well as from half-core measurements (Shipboard Scientific Party, 1995, 1996).

### Magnetostratigraphy

The polarity identification was based on declinations and inclinations. The time scale used is that of Berggren et al. (1995). In the deeper part, polarity interpretation was hampered by the extensive magnetic overprint on the inclinations, as mentioned above. The horizons between 145 and 148 mbsf at Hole 1083A, between 154 and 158 mbsf at Hole 1083B, and between 154 and 158 mbsf at Hole 1083D are indicative of a radial-inward remagnetization because they showed pre-orientation declinations close to zero. As a result, the beginning of the Olduvai Subchron was poorly constrained.

The Brunhes/Matuyama boundary (0.78 Ma) occurs at ~67 mbsf at Hole 1083A, at 60 mbsf at Hole 1083B, and at 68 mbsf at Hole 1083D (Fig. 5). The termination and beginning of the Jaramillo Subchron (C1r.1n), 0.99 and 1.07 Ma, respectively, occur at ~85 and 89 mbsf at Hole 1083A, at 78 and 84 mbsf at Hole 1083B, and at 86 and 92 mbsf at Hole 1083D. The termination and beginning of the Olduvai Chron (C2n), 1.77 and 1.95 Ma, respectively, occur at ~135 and

**Table 6. Overall diatom abundance estimated from smear slides and strewn slides of the 20- $\mu$ m fraction for Hole 1083A.**

Core, section, interval	Depth (mbsf)	Overall abundance (smear slide)	Overall abundance (sieved 20 $\mu$ m)	Dominant assemblage	Diatom stratigraphic zones	
175-1083A-						
1H-CC	1.74	3.0	3.0	Upw. + oceanic	NTD17	
2H-CC	9.22	1.0	5.0	Oceanic		
3H-CC	20.94	3.0	5.0	Upw. + oceanic		
5H-CC	40.19	1.0	4.0	<b>Neritic</b> + oceanic		
6H-CC	42.42	1.0	2.5			
7H-CC	59.08	2.0	3.0	Upwelling		
8H-CC	68.69	3.0	5.0	Upw. + oceanic		[ <i>P. curvirostris</i> ]
9H-CC	77.84	4.0	5.0	Upw. + oceanic		
10H-CC	87.6	1.5	3.0	Upw. + oceanic		
11H-CC	96.53	5.0	5.0			NTD16
12H-CC	106.66	3.0		neritic + oceanic		
13H-CC	115.19	3.5	5.0	Upw. + <b>oceanic</b>	[ <i>P. barboi</i> ]	
14H-CC	124.54	3.5	5.0	Oceanic		
15H-CC	134.79	4.0	5.0	Upw. + <b>oceanic</b>		
16H-CC	144.47	3.0	5.0	Oceanic		
17H-CC	154.12	5.0	5.0	Oceanic		
18H-CC	162.61	5.0		Upw. + oceanic		
19H-CC	173.22	5.0		Oceanic		
20H-CC	182.72	4.0	5.0	Upw. + oceanic		
21H-CC	192.23	4.0		Upw. + oceanic		
22H-CC	201.45	5.0		Upw. + <b>oceanic</b>		

Notes: Overall abundance is given as 0 = barren; 1 = trace; 2 = rare; 3 = few; 4 = common; and 5 = abundant. The dominant assemblage in each core catcher and the diatom stratigraphic zone (after Barron, 1985) are given. Note the occurrence of *Proboscia* (= *Simonseniella*) *curvirostris* in Sample 175-1083A-8H-CC and of *P. barboi* in Samples 15H-CC through 22H-CC.

144 mbsf at Hole 1083A, at 132 and 145 mbsf at Hole 1083B, and at 136 and 149 mbsf at Hole 1083D. The Matuyama/Gauss boundary (2.58 Ma) occurs at ~194 mbsf at Hole 1083A and at 192 mbsf at Hole 1083B. The bottom of Hole 1083D is estimated to be just at the Matuyama/Gauss boundary based on correlation of the remanent intensity between Holes 1083A and 1083D.

## COMPOSITE SECTION

At Site 1083, four holes were cored with a maximum penetration of 206.15 mbsf. Physical properties and color reflectance data were measured at 2-cm (Hole 1083A) and at 4-cm (Holes 1083B, 1083C, and 1083D) intervals. The correlation of features present in the physical and visual properties measurements of adjacent holes was used to demonstrate the completeness of the local stratigraphic sequence drilled and to establish a depth scale in terms of meters composite depth (mcd) for Site 1083. The continuity of the stratigraphic sequence could be demonstrated between 0 and 218.1 mcd, with a gap between 46 and 47.5 mcd (Fig. 8; Table 8).

At Site 1083, magnetic susceptibility and wet bulk density (GRAPE) were used to establish the mcd scale. The data sets were extensively processed before being used for correlation. Suspect measurements were eliminated by thresholding the data. The resulting data were smoothed using a Gaussian filter with a length of 12 cm. All data shown in Figures 8 and 9 were processed as described above.

The gap in the sedimentary sequence at 46 mcd results from only 28% recovery in Core 175-1083A-6H and 66% recovery in Core 175-1083B-5H. Stratigraphic correlation indicated that Cores 175-1083A-6H, 175-1083B-5H, and 175-1083D-5H (95% recovery) all

**Table 7. Tensor tool-orientation data for cores from Holes 1083A, 1083B, and 1083D.**

Core	MTF (°)	Inclination angle
175-1083A-		
4H	109	0.49
5H	8	0.50
6H	188	0.85
7H	167	0.79
8H	259	0.48
9H	293	0.57
10H	295	1.06
11H	345	0.88
12H	227	1.47
13H	118	1.02
14H	63	1.02
15H	292	0.84
16H	184	1.41
17H	341	1.16
18H	252	1.22
19H	47	1.16
20H	70	1.22
21H	308	1.09
22H	182	1.41
175-1083B-		
3H	322	0.32
4H	330	0.41
5H	249	0.28
6H	181	0.13
7H	285	0.09
8H	269	0.17
9H	38	0.33
10H	66	0.58
11H	129	0.31
12H	130	0.35
13H	78	0.49
14H	310	0.32
15H	154	0.47
16H	67	0.39
17H	235	0.56
18H	220	0.66
19H	159	0.93
20H	179	0.96
21H	98	0.83
22H	101	0.84
175-1083D-		
3H	153	1.02
4H	33	0.96
5H	342	0.91
6H	326	0.96
7H	140	1.09
8H	60	1.02
9H	75	1.05
10H	37	1.22
11H	110	1.40
12H	125	1.38
13H	91	1.46
14H	267	0.98
15H	297	1.56
16H	349	1.01
17H	18	0.88
18H	86	0.65
19H	6	1.01
20H	88	0.58
21H	7	1.01

Notes: The orientation parameter (MTF) is the angle in degrees between magnetic north and the double line marked on the center of the working half of the core. The local declination anomaly is 15°W.

end at the same depth. The length of the gap at 46 mcd between the two complete sections is unknown. Based on the driller's depth (in mbsf), at least 1.5 m of sediment are missing between Cores 175-1083D-5H and 6H.

Although Core 175-1083A-4H was recovered empty, the sedimentary sequence above 46 mcd is complete. Large gaps exist between Cores 175-1083A-1H and 2H (2.5 m), Cores 175-1083B-1H and 2H (6 m), Cores 175-1083B-2H and 3H (3 m), and Cores 175-1083B-4H and 5H (3 m). The most complete recovery is found at Hole 1083D.

The spliced record presented in Figure 9 and Table 9 is continuous to 46 mcd and from 47.5 to 218 mcd for magnetic susceptibility and

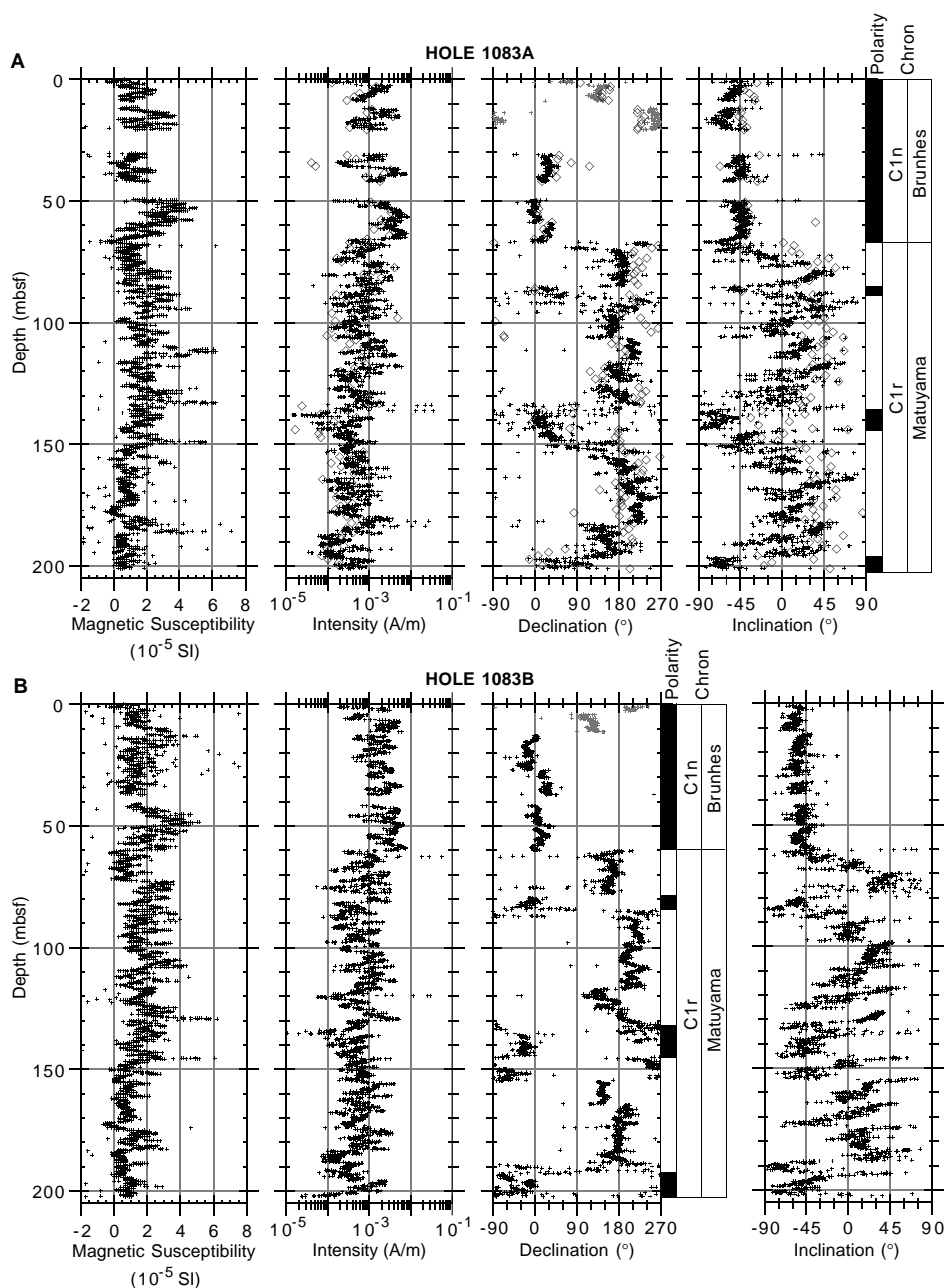


Figure 5. Magnetic susceptibility (SI) and NRM intensity, declination, magnetostratigraphic interpretation, and inclination after 20-mT demagnetization. Black symbols = Tensor corrected; gray symbols = uncorrected; open diamonds = discrete samples. Polarity shading: black = normal and white = reversed. **A.** Hole 1083A. **B.** Hole 1083B. (Continued on next page.)

GRAPE density. The selection of cores to be included in the spliced record and the placement of tie points were carried out mainly using the composite section of the magnetic susceptibility from Site 1083. Cores from Holes 1083A, 1083B, and 1083D had to be used in almost equal numbers to ensure completeness of the shipboard splice.

The resulting growth of the mcd scale compared with the standard ODP mbsf scale is ~13% (Section 175-1083B-21H-CC at 218 mcd and 192.8 mbsf). The growth of offsets applied to cores with meters below seafloor is not exactly linear (Fig. 10) but is always close to 10%. The offsets applied to cores from Hole 1083B are ~4 m larger because of an offset of 5.88 m applied to Core 175-1083B-2H.

## INORGANIC GEOCHEMISTRY

Fourteen interstitial water samples were gathered from Hole 1083A between 3.2 and 186.6 mbsf. Whole-round samples were sampled at a frequency of one sample per core to 101.1 mbsf and every third core thereafter to total depth (Table 10). Although the total penetration at Site 1083 was less than that at Sites 1081 and 1082, there are interesting similarities and contrasts among these three neighboring sites. In general, the interstitial water chemical trends at Site 1083 are intermediate between those at Sites 1081 and 1082.

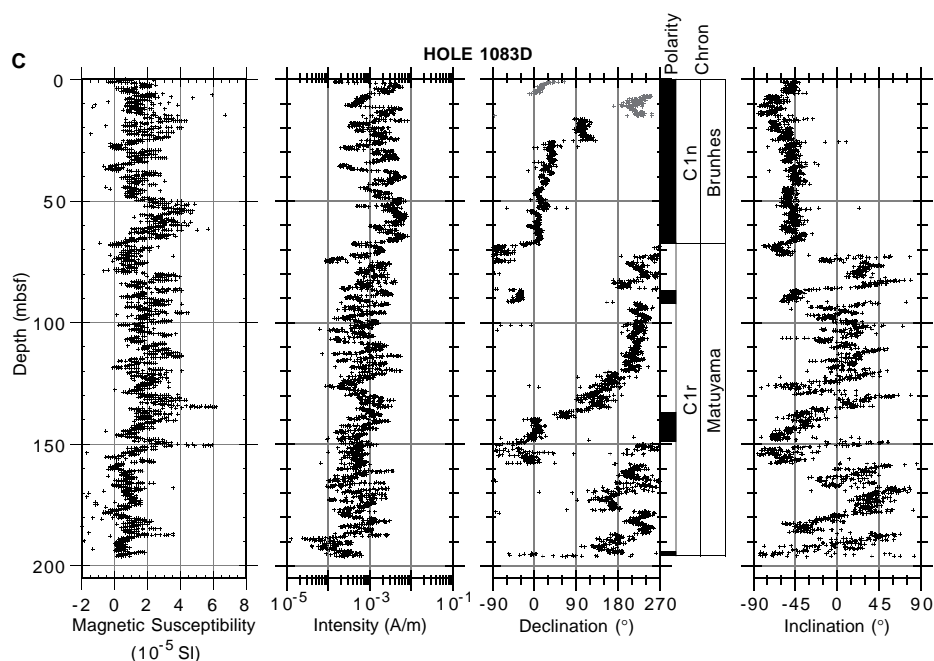


Figure 5 (continued). C. Hole 1083D.

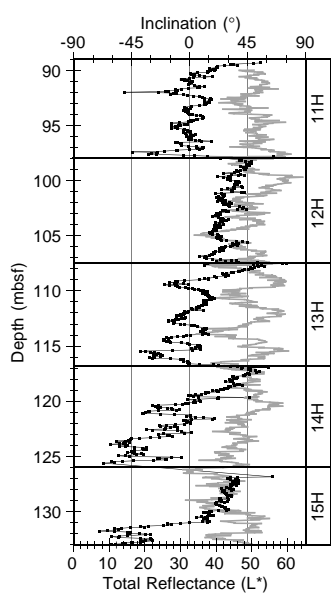


Figure 6. Inclinations of NRM (black line) and total reflectance of spectrophotometry (gray line) of Cores 175-1083B-11H through 15H. Note the downcore negative shift in inclination and the superimposed cyclic fluctuation correlated with the total reflectance.

### Alkalinity, Sulfate, and Ammonium

Downcore profiles of alkalinity, sulfate, and ammonium (Fig. 11) through the upper ~50 mbsf record the degradation of organic matter. Alkalinity increases to a maximum value of 37 mM at 63 mbsf, and ammonium records the greatest rate of increase through this depth range as well. The concentration of ammonium increases gradually to

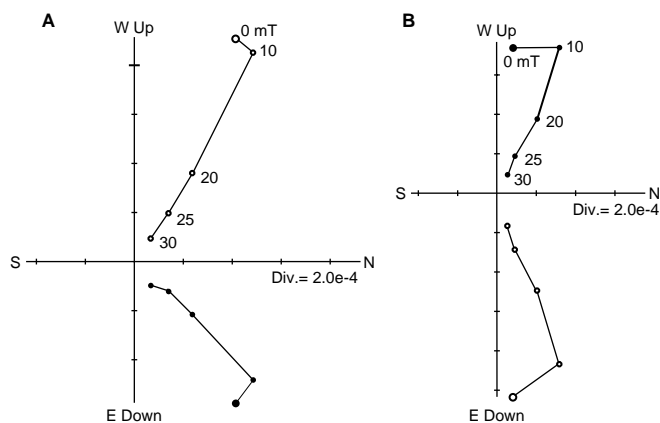


Figure 7. Orthogonal plots of progressive AF demagnetization data of discrete Samples (A) 175-1083A-5H-2, 100 cm, and (B) 175-1083A-13H-6, 59 cm, before orientation. Solid circles = projections of vector endpoints on the horizontal plane; open circles = projections of vector endpoints on the vertical plane.

a broad maximum at ~100 mbsf. Sulfate is completely consumed within the upper 35 mbsf, which is midway between the depth of sulfate depletion at Sites 1081 and 1082.

### Calcium, Magnesium, and Strontium

Concentration profiles of  $\text{Ca}^{2+}$ ,  $\text{Mg}^{2+}$ , and  $\text{Sr}^{2+}$  reflect the competing processes of carbonate dissolution and precipitation (Fig. 12). The concentration profiles of dissolved  $\text{Ca}^{2+}$  and  $\text{Mg}^{2+}$  are very similar to those observed at Sites 1081 and 1082 and largely reflect effects of carbonate precipitation including dolomitization. Dissolved  $\text{Sr}^{2+}$  increases to a maximum of ~500  $\mu\text{M}$  at the bottom of the hole. This

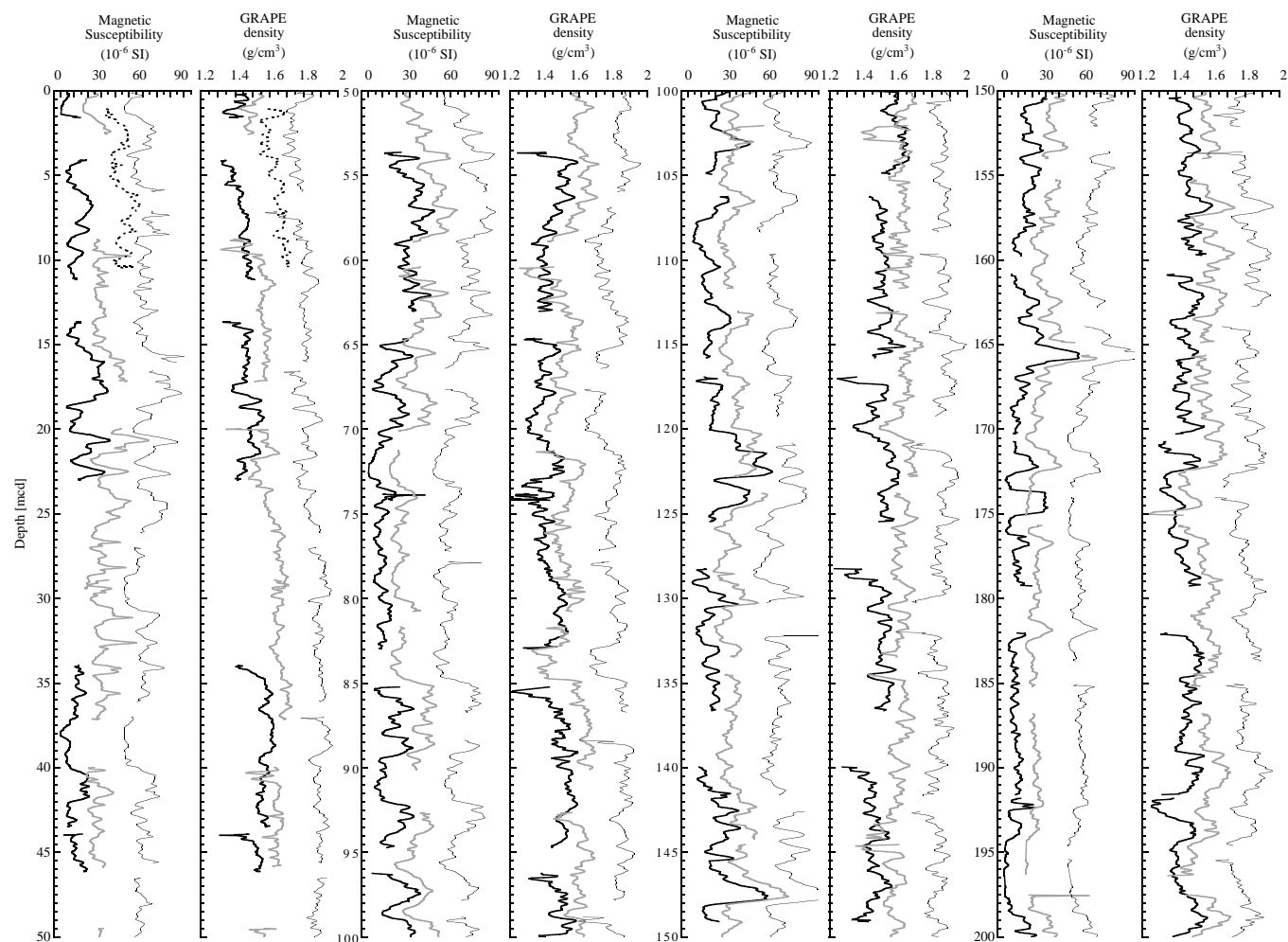


Figure 8. Composite section for Site 1083. Magnetic susceptibility and GRAPE density are plotted for Holes 1083A (thick black line), 1083B (gray line), 1083C (dashed line), and 1083D (thin black line). The downhole logs are shown in meters composite depth (mcd). Offsets have been applied for clarity.

concentration is 2–3 times higher than that observed at Sites 1081 and 1082, reflecting the greater availability of biogenic calcite at Site 1083.

### Silica and Phosphate

Dissolved silica is present in interstitial waters from Site 1083 at concentrations greater than representative bottom-water values (Fig. 13), indicating the dissolution of biogenic opal. Although the concentration of dissolved silica increases with depth, there is no obvious structure to the profile, other than a one-point maximum at Core 175-1083A-9H, a core that has a high abundance of diatoms (see “Biostratigraphy and Sedimentation Rates” section, this chapter). The concentration profile of dissolved silica at Site 1083 is not substantially different from profiles at Sites 1081 and 1082.

Dissolved phosphate concentrations increase with depth because of remineralization of organic matter. The increase closely follows that found at Site 1082, although the maximum value at Site 1083 is significantly less than that at Site 1082 (Fig. 13). Also, the rate of decrease in dissolved phosphate in deeper sediments at Site 1083 is greater than at Site 1082, reflecting a stronger uptake of dissolved phosphate into diagenetic phases.

### Sodium and Potassium

The concentration of dissolved  $\text{Na}^+$  increases from seawater values to maximum values at depth (Fig. 14). This distribution of dis-

solved  $\text{Na}^+$  is very similar to the distributions at Sites 1081 and 1082. The concentration of dissolved  $\text{K}^+$  remains essentially unchanged throughout the sequence.

### Salinity and Chloride

Consistent with the fact that the concentrations of many dissolved constituents at Site 1083 are intermediate to those at Sites 1081 and 1082, the salinity at Site 1083 also has intermediate values (Fig. 15). Concentrations of dissolved  $\text{Cl}^-$  steadily increase to the bottom of the hole.

## ORGANIC GEOCHEMISTRY

Calcium carbonate and organic carbon concentrations were measured on sediment samples from Hole 1083A (Table 11). Organic matter atomic carbon/nitrogen (C/N) ratios and Rock-Eval pyrolysis analyses were employed to determine the type of organic matter contained within the sediments. Elevated amounts of gas were encountered, and routine monitoring of the sedimentary gases was done for drilling safety.

### Inorganic and Organic Carbon Concentrations

Concentrations of carbonate carbon in Site 1083 sediments range between 9.9 and 2.4 wt%, corresponding to 82.8 and 19.8 wt%

**Table 8. Offsets applied to cores from Holes 1083A, 1083B, 1083C, and 1083D.**

Core	Depth (mbsf)	Offset (m)	Composite depth (mcd)
175-1083A-			
1H	0.0	0.10	0.10
2H	1.8	2.21	4.01
3H	11.3	2.30	13.60
5H	30.3	3.58	33.88
6H	39.8	4.05	43.85
7H	49.3	4.26	53.56
8H	58.8	5.75	64.55
9H	68.3	5.43	73.73
10H	77.8	7.37	85.17
11H	87.3	8.86	96.16
12H	96.8	9.35	106.15
13H	106.3	10.53	116.83
14H	115.8	12.35	128.15
15H	125.3	14.57	139.87
16H	134.8	15.51	150.31
17H	144.3	16.45	160.75
18H	153.8	16.85	170.65
19H	163.3	18.65	181.95
20H	172.8	18.91	191.71
21H	182.3	19.91	202.21
22H	191.8	20.37	212.17
175-1083B-			
1H	0.0	-0.10	-0.10
2H	2.8	5.88	8.68
3H	12.3	7.58	19.88
4H	21.8	7.02	28.82
5H	31.3	8.60	39.90
6H	40.8	8.60	49.40
7H	50.3	10.02	60.32
8H	59.8	11.38	71.18
9H	69.3	12.30	81.60
10H	78.8	13.77	92.57
11H	88.3	13.67	101.97
12H	97.8	15.15	112.95
13H	107.3	16.39	123.69
14H	116.8	17.59	134.39
15H	126.3	18.17	144.47
16H	135.8	19.35	155.15
17H	145.3	20.25	165.55
18H	154.8	20.79	175.59
19H	164.3	22.43	186.73
20H	173.8	23.63	197.43
21H	183.3	24.41	207.71
22H	192.8	25.79	218.59
175-1083C-			
1H	0.0	0.98	0.98
175-1083D-			
1H	0.0	0.00	0.00
2H	6.1	0.92	7.02
3H	15.6	0.84	16.44
4H	25.1	1.76	26.86
5H	34.6	2.30	36.90
6H	44.1	2.30	46.40
7H	53.6	3.18	56.78
8H	63.1	4.44	67.54
9H	72.6	5.12	77.72
10H	82.1	6.17	88.27
11H	91.6	7.13	98.73
12H	101.1	8.43	109.53
13H	110.6	10.15	120.75
14H	120.1	11.75	131.85
15H	129.6	12.89	142.49
16H	139.1	14.41	153.51
17H	148.6	15.23	163.83
18H	158.1	15.83	173.93
19H	167.6	17.37	184.97
20H	177.1	18.21	195.31
21H	186.6	18.93	205.53

Note: The offsets transform ODP standard depth values in meters below seafloor (mbsf) to meters composite depth (mcd).

CaCO<sub>3</sub> (Table 11). The carbonate concentrations display closely spaced changes related to light–dark color fluctuations (Fig. 16). Sediments at this site are divided into an upper lithostratigraphic subunit and a lower unit (see “Lithostratigraphy” section, this chapter). Subunit IA, a Pleistocene–Holocene foraminifer-rich clayey nannofossil ooze, averages 57 wt% CaCO<sub>3</sub>. Subunit IB is a Pliocene–Pleistocene diatom- and foraminifer-rich clayey nannofossil ooze that averages 50 wt% CaCO<sub>3</sub>. The variations in concentrations reflect varying combinations of changes in delivery of calcareous material, dilution by

noncalcareous components, and carbonate dissolution fueled by oxidation of organic matter.

Total organic carbon (TOC) determinations were done on selected samples of Hole 1083A sediments to estimate the amounts of organic matter in the two lithostratigraphic subunits (Table 11). Like CaCO<sub>3</sub> concentrations, TOC concentrations fluctuate on various scales (Fig. 17). Dark-colored sediments have higher TOC values than light-colored layers. TOC concentrations differ somewhat in Hole 1083A lithostratigraphic units, averaging 3.12 wt% in Subunit IA and 2.36 wt% in Subunit IB. The elevated TOC concentrations in the subunits are a consequence of the elevated paleoproductivity of the nearby Benguela Current upwelling system, which has delivered abundant organic matter to the sediments, and the high accumulation rate of sediments (see “Biostratigraphy and Sedimentation Rates” section, this chapter), which has enhanced preservation of the organic matter.

### Organic Matter Source Characterization

Organic C/N ratios were calculated for sediment samples from the different Site 1083 lithostratigraphic units using TOC and total nitrogen concentrations (Table 11). The C/N ratios vary from 17.4 to 8.2 (Fig. 18). These C/N ratios are intermediate between unaltered algal organic matter (5–8) and fresh land-plant material (25–35; e.g., Emerson and Hedges, 1988; Meyers, 1994). The mean C/N ratios of the two lithostratigraphic subunits are virtually identical (12.4 in Subunit IA and 12.6 in Subunit IB). Because of their setting seaward of a major upwelling system and offshore from a coastal desert, it is likely that these sediments contain mostly marine-derived organic matter with only a minor contribution of detrital continental organic matter. The C/N ratios indicate that preferential loss of nitrogen-rich, proteinaceous matter and consequent elevation of C/N ratios occurred during settling of organic matter to the seafloor. Such early diagenetic alteration of C/N ratios is often seen under areas of elevated marine productivity such as upwelling systems (Meyers, 1997).

A Van Krevelen–type plot of the hydrogen index (HI) and oxygen index (OI) values indicates that the sediments contain type II (algal) organic matter (Fig. 19) that has been altered by microbial processing during early diagenesis. Well-preserved type II organic matter has high HI values (Peters, 1986); these values can be lowered by microbial oxidation (Meyers, 1997). In general, Hole 1083A sediments having lower Rock-Eval TOC values also have lower HI values (Fig. 20). This relationship confirms that the marine organic matter has been subject to partial oxidation, which simultaneously lowers TOC and HI values (Meyers, 1997). Further evidence of substantial amounts of in situ organic matter degradation exists in the large decreases in sulfate and increases in alkalinity and ammonia in the interstitial waters of Site 1083 sediments (see “Inorganic Geochemistry” section, this chapter).

The sediment samples have low Rock-Eval T<sub>max</sub> values (Table 12), showing that their organic matter is thermally immature with respect to petroleum generation (Peters, 1986) and therefore is unlikely to contain much detrital organic matter derived from erosion of ancient sediments from Africa.

### Headspace Gases

Relatively high amounts of hydrogen sulfide, methane, and CO<sub>2</sub> were found in sediments from Site 1083. The odor of hydrogen sulfide was noted in Cores 175-1083A-2H through 15H (3.3–130 mbsf). Total gas pressures became great enough in sediments below Core 3H (18 mbsf) to require perforating the core liner to relieve the pressure and prevent excessive core expansion.

Methane (C<sub>1</sub>) first appears in headspace gas samples of Hole 1083A sediments at 6.3 mbsf. Concentrations become significant in sediments below 35 mbsf (Fig. 21). As at Sites 1081 and 1082, high methane/ethane (C<sub>1</sub>/C<sub>2</sub>) ratios and the absence of major contributions of higher molecular weight hydrocarbon gases (Table 13) indicate that the gas is biogenic, as opposed to thermogenic, in origin. A bio-

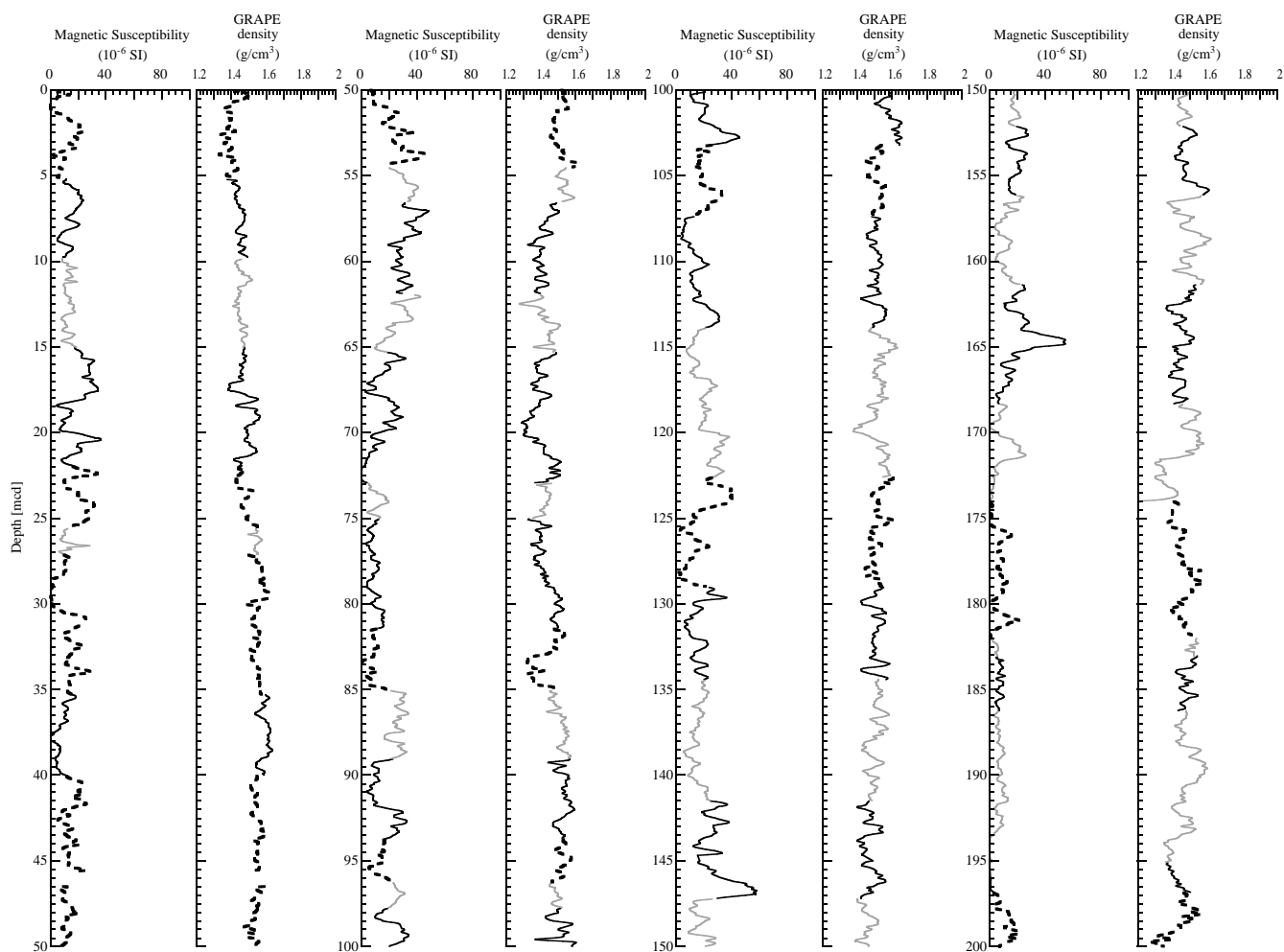


Figure 9. Spliced records for magnetic susceptibility and GRAPE density plotted in meters composite depth (mcd). Cores from Holes 1083A, 1083B, and 1083D have been used for the spliced record: solid black line = Hole 1083A, gray line = Hole 1083B, and dashed line = Hole 1083D.

genic origin of the methane is supported by the disappearance of interstitial sulfate at approximately the same sub-bottom depth where methane concentrations begin to rise (see “Inorganic Geochemistry” section, this chapter), inasmuch as Claypool and Kvenvolden (1983) observe that the presence of interstitial sulfate inhibits microbial methanogenesis in marine sediments.

Natural gas analyses determined that the most abundant gas was  $\text{CO}_2$ , and that headspace concentrations of this gas remained high deep in Hole 1083A (200 mbsf; Fig. 22). Cragg et al. (1992) isolated viable microbes to depths of ~500 mbsf in sediments of the Japan Sea. The abundance of biogenic gases in sediments from Site 1083 suggests the presence of similarly viable microbial communities throughout the sedimentary sequence at this location.

## PHYSICAL PROPERTIES

Physical properties measurements at Hole 1083A included measurements with the MST on whole-round sections of cores from each hole. Discrete velocities, index properties, vane-shear, and thermal conductivity measurements were conducted on half-split cores (see “Explanatory Notes” chapter, this volume).

Index properties (gravimetric wet bulk density, porosity, and moisture content) were generally determined on one or two samples (volume = ~10  $\text{cm}^3$ ) per working-half section on all cores from Hole

1083A. Method C was used at this site (see “Explanatory Notes” chapter, this volume).

Compressional ( $P$ -wave) velocity and undrained vane shear strength measurements were made at a resolution of one or two sampling points per section. For discrete  $P$ -wave velocity measurements, the modified Hamilton Frame was used. Thermal conductivity was obtained on every second section in every core from Hole 1083A by inserting a probe into the unsplit core (see “Explanatory Notes” chapter, this volume).

## Multisensor Track

GRAPE density (Fig. 23),  $P$ -wave velocity (Fig. 24), and magnetic susceptibility (Fig. 25A) were determined every 2 cm for the first 10 cores (0–85 mbsf). MST data are included on CD-ROM (back pocket, this volume). Below 85 mbsf, the resolution was reduced to 4 cm. Compressional velocities were recorded at an amplitude threshold of 100 incremental units to exclude weaker signals. The MST  $P$ -wave logger did not record any signals below 125 mbsf (Fig. 24). In general, MST velocities and discrete velocities seem to correlate in some intervals between 0 and 125 mbsf. MST  $P$ -wave values appear to be lower than discrete velocity values over the entire depth range.

Magnetic susceptibility (Fig. 25A) and GRAPE density (Fig. 23) show a high correlation over the entire depth range of 200 m. Index

**Table 9. List of splice tie points used to create the continuous “spliced” stratigraphic sequence for Site 1083.**

Hole, core, section, interval (cm)	Depth (mbsf)	Composite depth (mcd)	Whether tied	Hole, core, section, interval (cm)	Depth (mbsf)	Composite depth (mcd)	Offset (m)
1083D-1H-4, 72	5.22	5.22	Tie to	1083A-2H-2, 4	3.34	5.22	1.88
1083A-2H-5, 10	7.90	9.78	Tie to	1083B-2H-1, 144	4.24	9.78	5.54
1083B-2H-5, 68	9.48	15.02	Tie to	1083A-3H-2, 16	12.96	15.02	2.06
1083A-3H-6, 108	19.88	21.94	Tie to	1083D-3H-4, 124	21.34	21.94	0.60
1083D-3H-7, 36	24.96	25.56	Tie to	1083B-3H-4, 124	18.04	25.56	7.52
1083B-3H-5, 128	19.58	27.10	Tie to	1083D-4H-1, 36	25.46	27.10	1.64
1083D-4H-6, 104	33.64	35.28	Tie to	1083A-5H-2, 4	31.84	35.28	3.44
1083A-5H-5, 36	36.56	40.00	Tie to	1083D-5H-3, 12	37.72	40.00	2.28
1083D-5H-6, 1200	43.30	45.58	Tie to	1083D-6H-1, 0	44.10	46.40	2.30
1083D-6H-6, 60	52.20	54.50	Tie to	1083B-6H-4, 88	45.90	54.50	8.60
1083B-6H-5, 140	47.92	56.52	Tie to	1083A-7H-2, 146	52.26	56.52	4.26
1083A-7H-6, 92	57.62	61.88	Tie to	1083B-7H-1, 144	51.74	61.88	10.14
1083B-7H-4, 36	55.16	65.30	Tie to	1083A-8H-1, 76	59.56	65.30	5.74
1083A-8H-6, 98	67.18	72.92	Tie to	1083B-8H-2, 24	61.54	72.92	11.38
1083B-8H-3, 84	63.64	75.02	Tie to	1083A-9H-1, 126	69.56	75.02	5.46
1083A-9H-6, 26	75.96	81.42	Tie to	1083D-9H-3, 56	76.16	81.42	5.26
1083D-9H-5, 116	79.76	85.02	Tie to	1083B-9H-3, 36	72.66	85.02	12.36
1083B-9H-5, 136	76.66	89.02	Tie to	1083A-10H-3, 102	81.82	89.02	7.20
1083A-10H-6, 132	86.52	93.72	Tie to	1083D-10H-4, 116	87.76	93.72	5.96
1083D-10H-6, 68	90.28	96.24	Tie to	1083B-10H-3, 104	82.84	96.24	13.40
1083B-10H-4, 104	84.34	97.74	Tie to	1083A-11H-2, 40	89.23	97.74	8.51
1083A-11H-6, 16	94.68	103.19	Tie to	1083D-11H-4, 20	96.30	103.19	6.89
1083D-11H-6, 136	100.46	107.35	Tie to	1083A-12H-1, 140	98.20	107.35	9.15
1083A-12H-6, 52	104.72	113.87	Tie to	1083B-12H-1, 96	98.76	113.87	15.11
1083B-12H-7, 68	107.48	122.59	Tie to	1083D-13H-2, 52	112.62	122.59	9.97
1083D-13H-6, 92	119.02	128.99	Tie to	1083A-14H-2, 4	117.34	128.99	11.65
1083A-14H-5, 96	122.76	134.41	Tie to	1083B-14H-1, 60	117.40	134.41	17.01
1083B-14H-6, 16	124.46	141.47	Tie to	1083A-15H-2, 92	127.72	141.47	13.75
1083A-15H-6, 72	133.42	147.17	Tie to	1083B-15H-3, 44	129.74	147.17	17.43
1083B-15H-6, 88	134.68	152.11	Tie to	1083A-16H-2, 120	137.50	152.11	14.61
1083A-16H-5, 72	141.52	156.13	Tie to	1083B-16H-2, 36	137.66	156.13	18.47
1083B-16H-5, 108	142.88	161.35	Tie to	1083A-17H-2, 4	145.84	161.35	15.51
1083A-17H-6, 100	152.80	168.31	Tie to	1083B-17H-3, 60	148.90	168.31	19.41
1083B-17H-7, 28	154.58	173.99	Tie to	1083D-18H-1, 88	158.98	173.99	15.01
1083D-18H-6, 136	166.96	181.97	Tie to	1083B-18H-5, 132	162.12	181.97	19.85
1083B-18H-6, 84	163.14	182.99	Tie to	1083A-19H-2, 36	165.16	182.99	17.83
1083A-19H-4, 60	168.40	186.23	Tie to	1083B-19H-1, 20	164.50	186.23	21.73
1083B-19H-7, 4	173.34	195.07	Tie to	1083A-20H-3, 128	177.08	195.07	17.99
1083A-20H-5, 4	178.84	196.83	Tie to	1083D-20H-2, 76	179.36	196.83	17.47
1083D-20H-7, 4	186.14	203.61	Tie to	1083B-20H-5, 88	180.68	203.61	22.93
1083B-20H-7, 28	183.08	206.01	Tie to	1083A-21H-4, 12	186.92	206.01	19.09
1083A-21H-6, 124	191.04	210.13	Tie to	1083B-21H-2, 140	186.20	210.13	23.93
1083B-21H-7, 4	192.34	216.27	Tie to	1083A-22H-4, 60	196.90	216.27	19.37
1083A-22H-6, 64	199.94	219.31	Tie to	1083B-22H-2, 4	194.34	219.31	24.97
1083B-22H-7, 64	202.44	227.41					

Note: The tie points are listed in standard ODP meters below seafloor (mbsf) and meters composite depth (mcd).

properties wet bulk density values follow the GRAPE density profile over the entire depth range. Because only minor cracks and voids in the sediments were observed at Hole 1083A, both data sets correspond to each other very well. GRAPE density and wet bulk density values display a higher overall variation between 0 and 70 mbsf than below 70 mbsf.

All physical properties data sets reveal clear and pronounced cyclicities, which will be subject to further detailed analyses on shore. However, thorough editing will be required to correct for different types of deformation within cores and between holes.

### Velocities

Discrete velocities range between 1520 and 1590 m/s between 0 and 200 mbsf. The *P*-wave logger of the MST recorded lower values from 0 to 125 mbsf (Fig. 24). At depths of 4, 32, and 83 mbsf, high-velocity peaks are noticed. Wet bulk and GRAPE density profiles show a sharp positive density gradient only at ~115 mbsf (Fig. 23). Density and velocity profiles correspond to each other between 5 and 50 mbsf and for most of the depth interval between 135 and 200 mbsf, but show a negative correlation in other depth intervals.

### Index Properties

Results of discrete measurements of wet bulk density, porosity, and moisture content are illustrated in Figures 26A, 26B, and 26C, respectively (also see Table 14 on CD-ROM, back pocket, this vol-

ume). The density values vary between 1250 and 1800 kg/m<sup>3</sup>. The overall trend of the wet bulk density profile shows increasing values in the upper 50 m and significant variability below this depth. Below 50 mbsf, a decrease in wet bulk density can be noticed, with a minimum at 65 mbsf (corresponding to a local velocity maximum). At 115 mbsf, the highest density value for Hole 1083A is found (1680 kg/m<sup>3</sup>). Density decreases slightly below a depth of 115 mbsf, but variations confirm that small-scale cycles are present, as observed in GRAPE density and magnetic susceptibility core logs.

In general, porosity and moisture profiles show the expected inverse correlation with the wet bulk density curve. Porosities decrease from 82% in the top section to lowest values of 65% (Fig. 26B). Moisture content varies between 65% at the top of Hole 1083A and 42% (Fig. 26C).

### Thermal Conductivity

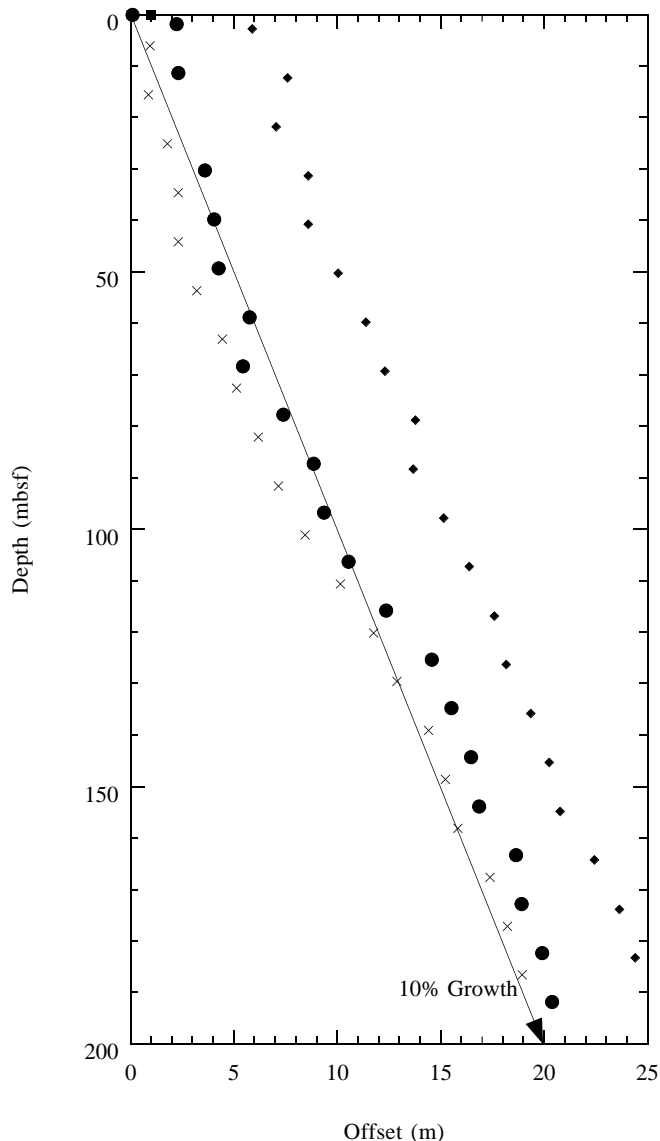
The thermal conductivity profile (Fig. 25B) at Hole 1083A was measured in every second core section (see “Explanatory Notes” chapter, this volume). The profile is similar to wet bulk and GRAPE density profiles over most of the depth range at Hole 1083A (Fig. 23).

### Vane Shear Strength

Undrained vane-shear measurements were performed in the bottom part of each core section. The profile between 0 and 200 mbsf shows little variation in vane shear strength from the top of Hole

Site 1083 Offsets

REFERENCES



Barron, J.A., 1985. Late Eocene to Holocene diatom biostratigraphy of the equatorial Pacific Ocean, Deep Sea Drilling Project Leg 85. *In* Mayer, L., Theyer, F., Thomas, E., et al., *Init. Repts. DSDP*, 85: Washington (U.S. Govt. Printing Office), 413–456.

Berggren, W.A., Kent, D.V., Swisher, C.C., III, and Aubry, M.-P., 1995. A revised Cenozoic geochronology and chronostratigraphy. *In* Berggren, W.A., Kent, D.V., Aubry, M.-P., and Hardenbol, J. (Eds.), *Geochronology, Time Scales and Global Stratigraphic Correlation*. Spec. Publ.—Soc. Econ. Paleontol. Mineral. (Soc. Sediment. Geol.), 54:129–212.

Caulet, J.-P., 1991. Radiolarians from the Kerguelen Plateau, Leg 119. *In* Barron, J., Larsen, B., et al., *Proc. ODP, Sci. Results*, 119: College Station, TX (Ocean Drilling Program), 513–546.

Claypool, G.E., and Kvenvolden, K.A., 1983. Methane and other hydrocarbon gases in marine sediment. *Annu. Rev. Earth Planet. Sci.*, 11:299–327.

Cragg, B.A., Harvey, S.M., Fry, J.C., Herbert, R.A., and Parkes, R.J., 1992. Bacterial biomass and activity in the deep sediment layers of the Japan Sea, Hole 798B. *In* Pisciotto, K.A., Ingle, J.C., Jr., von Breyman, M.T., Barron, J., et al., *Proc. ODP, Sci. Results*, 127/128 (Pt. 1): College Station, TX (Ocean Drilling Program), 761–776.

Emerson, S., and Hedges, J.I., 1988. Processes controlling the organic carbon content of open ocean sediments. *Paleoceanography*, 3:621–634.

Martini, E., 1971. Standard Tertiary and Quaternary calcareous nannoplankton zonation. *In* Farinacci, A. (Ed.), *Proc. 2nd Int. Conf. Planktonic Microfossils Roma*: Rome (Ed. Tecnosci.), 2:739–785.

Meyers, P.A., 1994. Preservation of elemental and isotopic source identification of sedimentary organic matter. *Chem. Geol.*, 144:289–302.

———, 1997. Organic geochemical proxies of paleoceanographic, paleolimnologic, and paleoclimatic processes. *Org. Geochem.*, 27:213–250.

Millero, F.J., and Sohn, M.L., 1992. *Chemical Oceanography*: Boca Raton (CRC Press).

Moore, T.C., Jr., 1995. Radiolarian stratigraphy, Leg 138. *In* Pisias, N.G., Mayer, L.A., Janecek, T.R., Palmer-Julson, A., and van Andel, T.H. (Eds.), *Proc. ODP, Sci. Results*, 138: College Station, TX (Ocean Drilling Program), 191–232.

Okada, H., and Bukry, D., 1980. Supplementary modification and introduction of code numbers to the low-latitude coccolith biostratigraphic zonation (Bukry, 1973; 1975). *Mar. Micropaleontol.*, 5:321–325.

Peters, K.E., 1986. Guidelines for evaluating petroleum source rock using programmed pyrolysis. *AAPG Bull.*, 70:318–329.

Shipboard Scientific Party, 1995. Site 926. *In* Curry, W.B., Shackleton, N.J., Richter, C., et al., *Proc. ODP, Init. Repts.*, 154: College Station, TX (Ocean Drilling Program), 153–232.

———, 1996. Explanatory notes. *In* Comas, M.C., Zahn, R., Klaus, A., et al., *Proc. ODP, Init. Repts.*, 161: College Station, TX (Ocean Drilling Program), 21–49.

Figure 10. Offsets applied to Site 1083 cores plotted against standard ODP meters below seafloor (mbsf). A linear 10% growth of meters composite depth (mcd) compared with mbsf is indicated by an arrow. Offsets are plotted for Hole 1083A (circles), Hole 1083B (diamonds), and Hole 1083D (crosses).

1083A to 200 mbsf, except between 55 and 65 mbsf. The shear strength increases slightly over the entire depth range at Hole 1083A. As observed at previous sites, local maxima in shear strength are usually observed in the middle of each core at Site 1083. Lower values coincide mostly with the top and the bottom of each core where gas expansion may have changed the sediment structure significantly.

Ms 175IR-111

**NOTE: Core-description forms (“barrel sheets”) and core photographs can be found in Section 4, beginning on page 581. Forms containing smear-slide data can be found on CD-ROM. See Table of Contents for materials contained on CD-ROM.**

**Table 10. Interstitial water composition for Hole 1083A.**

Core, section, interval (cm)	Depth (mbsf)	pH	Alkalinity (mM)	Salinity	Cl <sup>-</sup> (titr) (mM)	Cl <sup>-</sup> (IC) (mM)	SO <sub>4</sub> <sup>2-</sup> (mM)	Na <sup>+</sup> (mM)	Mg <sup>2+</sup> (mM)	Ca <sup>2+</sup> (mM)	K <sup>+</sup> (mM)	H <sub>4</sub> SiO <sub>4</sub> (μM)	NH <sub>4</sub> <sup>+</sup> (μM)	PO <sub>4</sub> <sup>3-</sup> (μM)	Sr <sup>2+</sup> (μM)
175-1083A-															
2H-1, 140-150	3.20	7.45	4.950	35.0	556	558	27.93	480	52.44	10.18	11.41	693	497	14	92
2H-3, 140-150	6.20	7.81	9.080	35.0	558	552	23.37	476	54.37	8.92	11.73	827	1234	32	93
3H-2, 140-150	14.20	7.83	18.400	35.0	562	587	14.83	472	55.99	6.55	12.50	812	3031	64	95
5H-3, 130-140	34.60	7.79	29.530	35.0	574	571	0.20	487	49.62	2.90	11.63	750	5194	78	137
6H-1, 140-150	41.20	7.31	35.090	35.0	574	573	0.25	495	48.14	3.08	11.73	760	5764	87	168
7H-3, 130-140	53.60	7.54	36.600	35.0	574	580	0.00	492	49.44	3.43	12.50	834	6683	122	198
8H-3, 130-140	63.10	6.95	37.040	35.5	574	579	0.04	497	47.67	3.19	11.76	815	7118	120	212
9H-3, 130-140	72.60	7.60	34.460	35.5	573	573	0.00	495	46.98	3.17	11.81	1053	7570	109	226
10H-3, 130-140	82.10	7.81	34.970	35.5	575	575	0.00	500	45.54	3.23	11.92	805	7926	87	243
11H-2, 145-155	90.28	7.79	33.420	35.0	572	576	0.00	502	41.68	3.64	12.33	1012	8077	76	256
12H-3, 130-140	101.10	7.80	30.890	35.0	582	576	0.00	510	41.28	3.57	12.61	1103	8655	57	282
15H-3, 130-140	129.60	7.20	26.810	35.0	586	595	0.00	517	37.67	3.77	12.39	1160	8718	34	333
18H-3, 130-140	158.10	7.35	28.190	35.0	591	596	0.00	520	37.09	6.17	11.93	1176	8283	28	405
21H-3, 130-140	186.60	7.81	24.557	35.5	596	605	0.00	526	35.93	4.63	13.51	1200	7982	20	482

Note: Cl<sup>-</sup> (titr) = analyzed by titration and Cl<sup>-</sup> (IC) = analyzed by ion chromatography.

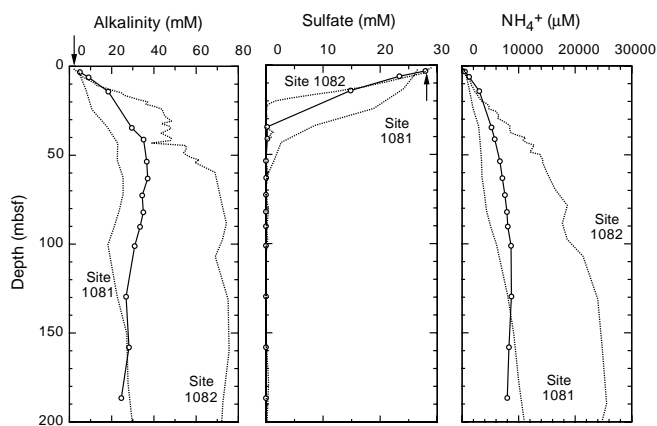


Figure 11. Downcore profiles of dissolved alkalinity, sulfate, and ammonium at Site 1083 (solid lines with open circles). Profiles for Sites 1081 and 1082 (dotted lines) are shown for comparison. Arrows = mean ocean-bottom-water values taken from Millero and Sohn (1992).

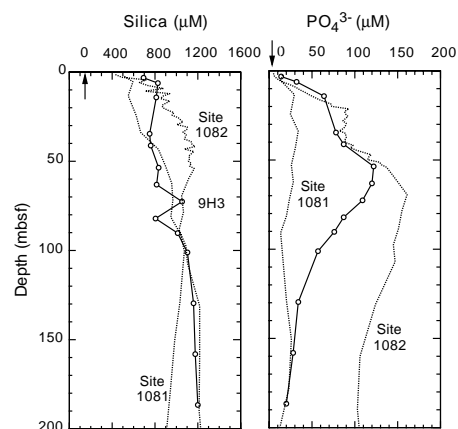


Figure 13. Downcore profiles of dissolved silica and phosphate at Site 1083 (solid lines with open circles). Profiles for Sites 1081 and 1082 (dotted lines) are shown for comparison. Position of Section 175-1083A-9H-3 indicated (see text). Arrows = mean ocean-bottom-water values taken from Millero and Sohn (1992).

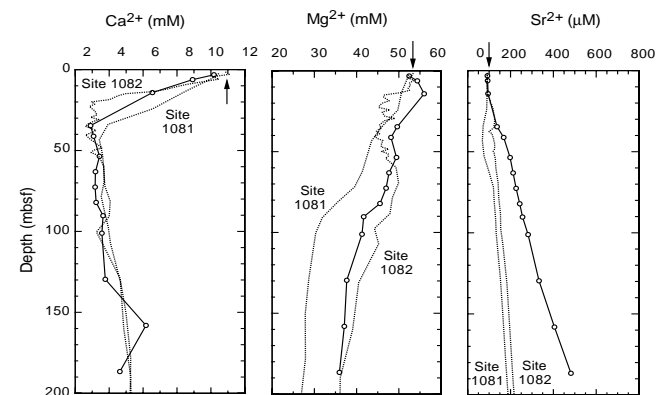


Figure 12. Downcore profiles of Ca<sup>2+</sup>, Mg<sup>2+</sup>, and Sr<sup>2+</sup> at Site 1083 (solid lines with open circles). Profiles for Sites 1081 and 1082 (dotted lines) are shown for comparison. Arrows = mean ocean-bottom-water values taken from Millero and Sohn (1992).

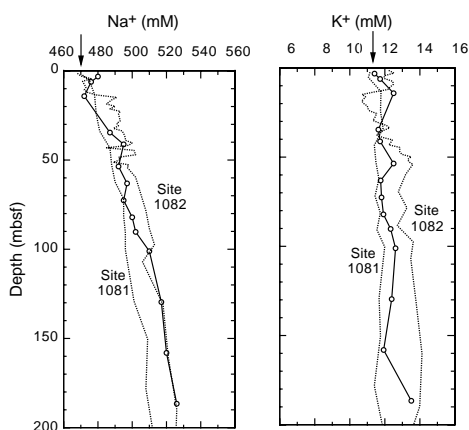


Figure 14. Downcore profiles of dissolved Na<sup>+</sup> and K<sup>+</sup> at Site 1083 (solid lines with open circles). Profiles for Site 1081 and 1082 (dotted lines) are shown for comparison. Arrows = mean ocean-bottom-water values taken from Millero and Sohn (1992).

**Table 11. Percentages of inorganic and total carbon, total nitrogen, and total sulfur in sediment samples from Hole 1083A.**

Core, section, interval (cm)	Depth (mbsf)	IC (wt%)	CaCO <sub>3</sub> (wt%)	TC (wt%)	TOC (wt%)	TN (wt%)	TS (wt%)	C/N (atomic)
175-1083A-								
Subunit IA - Pleistocene-Holocene foraminifer-rich clayey nannofossil ooze								
1H-1, 46-47	0.46	9.23	76.8	10.26	1.04	0.15	0.20	8.2
2H-1, 46-47	2.26	7.40	61.7	10.58	3.17	0.31	0.21	11.9
2H-3, 46-47	5.26	7.31	60.9	9.51	2.20	0.24	0.82	10.6
2H-5, 46-47	8.26	8.59	71.6					
3H-1, 46-47	11.76	8.31	69.2					
3H-3, 46-47	14.76	6.18	51.4	10.65	4.47	0.38	0.78	13.7
3H-5, 46-47	17.76	7.70	64.1					
5H-2, 46-47	32.26	9.16	76.3					
5H-4, 46-47	35.16	9.94	82.8	10.66	0.72	0.09	0.28	9.4
5H-6, 46-47	38.16	7.83	65.2					
6H-2, 46-47	41.76	8.48	70.7	10.98	2.49	0.22	0.96	13.0
7H-2, 46-47	51.26	5.89	49.1					
7H-4, 46-47	54.16	4.25	35.4	8.82	4.57	0.39	2.13	13.6
7H-6, 46-47	57.16	3.98	33.2					
8H-2, 45-46	60.75	4.20	35.0					
8H-4, 45-46	63.65	2.03	16.9	8.83	6.80	0.51	2.61	15.5
8H-6, 45-46	66.65	9.69	80.7					
9H-2, 45-46	70.25	8.07	67.2					
9H-4, 45-46	73.15	7.82	65.2	9.64	1.81	0.17	0.60	12.8
9H-6, 45-46	76.15	8.90	74.2					
10H-2, 45-46	79.75	6.96	58.0					
10H-4, 45-46	82.65	7.43	61.9	10.94	3.52	0.30	0.76	13.9
10H-6, 45-46	85.65	4.02	33.4					
11H-2, 45-46	89.28	6.82	56.8					
11H-4, 45-46	91.86	8.57	71.4	9.76	1.19	0.13	0.82	10.5
11H-6, 45-46	94.97	7.21	60.0					
12H-2, 45-46	98.75	8.66	72.1					
12H-4, 45-46	101.65	8.28	69.0	9.50	1.22	0.12	0.32	11.6
12H-6, 45-46	104.65	5.74	47.8					
13H-2, 45-46	108.25	6.21	51.7					
13H-4, 45-46	111.25	6.71	55.9	8.26	1.55	0.19	1.03	9.4
13H-6, 45-46	114.25	6.88	57.3					
14H-2, 45-46	117.75	7.30	60.8					
14H-4, 45-46	120.75	5.03	41.9	9.51	4.48	0.32	1.74	16.2
14H-6, 45-46	123.75	6.35	52.9					
15H-2, 45-46	127.25	5.32	44.3					
15H-4, 45-46	130.15	4.82	40.1					
15H-6, 45-46	133.15	2.38	19.8	9.92	7.54	0.57	3.29	15.5
Subunit IB - Pliocene-Pleistocene diatom- and foraminifer-rich clayey nannofossil ooze								
16H-2, 45-46	136.75	5.65	47.0					
16H-4, 45-46	139.75	5.32	44.3					
16H-6, 45-46	142.75	6.58	54.8	7.90	1.33	0.17	0.65	9.2
17H-2, 45-46	146.25	6.26	52.1					
17H-4, 45-46	149.25	3.22	26.9	8.39	5.17	0.41	3.06	14.7
17H-6, 45-46	152.25	5.72	47.7	7.22	1.50	0.14	0.72	12.3
18H-2, 46-47	155.76	4.18	34.8					
18H-4, 46-47	158.66	5.51	45.9	7.48	1.97	0.18	0.75	12.8
18H-6, 46-47	161.66	6.92	57.7					
19H-2, 46-47	165.26	6.73	56.0					
19H-4, 46-47	168.26	6.70	55.8	8.20	1.50	0.16	0.67	11.3
19H-6, 46-47	171.26	7.27	60.5					
20H-2, 46-47	174.76	7.32	61.0	8.64	1.31	0.14	0.29	10.8
20H-4, 46-47	177.76	6.83	56.9	8.05	1.23	0.12	0.31	12.1
20H-5, 60-61	179.40	7.65	63.8	8.88	1.23	0.14	0.47	10.6
20H-5, 100-101	179.80	8.19	68.2	9.30	1.11	0.12	0.62	10.5
20H-5, 144-145	180.24	7.30	60.8	9.43	2.14	0.20	0.53	12.4
20H-6, 4-5	180.34	6.79	56.5	8.98	2.19	0.21	1.11	12.0
20H-6, 46-47	180.76	6.71	55.9	8.80	2.10	0.20	0.88	12.3
20H-6, 80-81	181.10	2.93	24.4	8.45	5.52	0.40	2.21	16.3
20H-6, 120-121	181.50	3.12	26.0	8.05	4.93	0.33	2.21	17.4
20H-6, 144-145	181.74	3.43	28.5	7.35	3.92	0.31	1.66	14.7
20H-7, 19-20	181.99	4.89	40.7	7.65	2.76	0.22	1.07	14.4
20H-7, 60-61	182.40	6.31	52.6	8.68	2.37	0.21	1.06	13.1
21H-2, 46-47	184.26	6.65	55.4					
21H-4, 46-47	187.26	7.61	63.4	8.63	1.02	0.11	0.31	10.5
21H-6, 46-47	190.26	5.56	46.4					
22H-2, 46-47	193.76	5.36	44.6					
22H-4, 46-47	196.76	6.38	53.1					
22H-6, 46-47	199.76	5.54	46.2	7.00	1.46	0.15	0.59	11.7

Notes: IC = inorganic carbon; CaCO<sub>3</sub> = calcium carbonate; TC = total carbon; TOC = total organic carbon; TN = total nitrogen; TS = total sulfur; and C/N = carbon/nitrogen ratio. TOC concentrations are calculated from the difference between IC and TC concentrations. C/N ratios are calculated from TOC and TN concentrations and are given as atom/atom ratios.

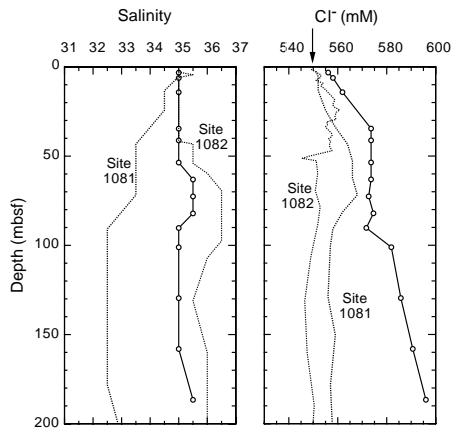


Figure 15. Downcore profiles of salinity and dissolved  $\text{Cl}^-$  at Site 1083 (solid lines with open circles). Profiles for Sites 1081 and 1082 (dotted lines) are shown for comparison. Arrow = mean ocean-bottom-water value taken from Millero and Sohn (1992).

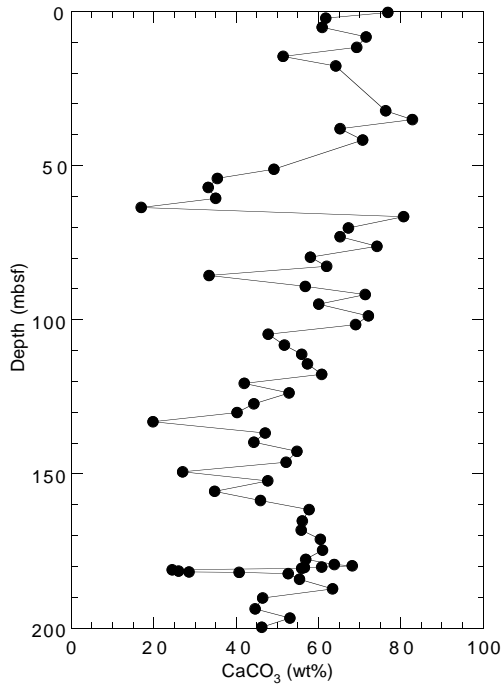


Figure 16. Concentrations of  $\text{CaCO}_3$  in sediments from Hole 1083A. Variations reflect light–dark color cycles.

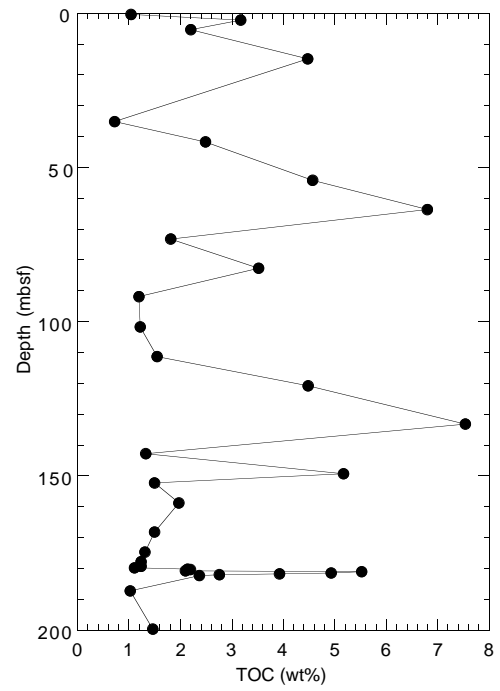


Figure 17. Concentrations of TOC in sediments from Hole 1083A. Variations reflect light–dark color cycles.

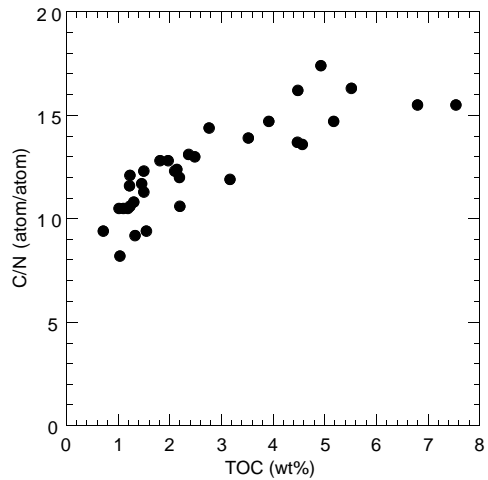


Figure 18. Comparison of organic matter C/N ratios and TOC concentrations of sediments from Hole 1083A. The correspondence between increases in both parameters indicates that preservation of marine organic matter during early diagenesis is important to enhancing the organic carbon richness of sediments near the Walvis Ridge.

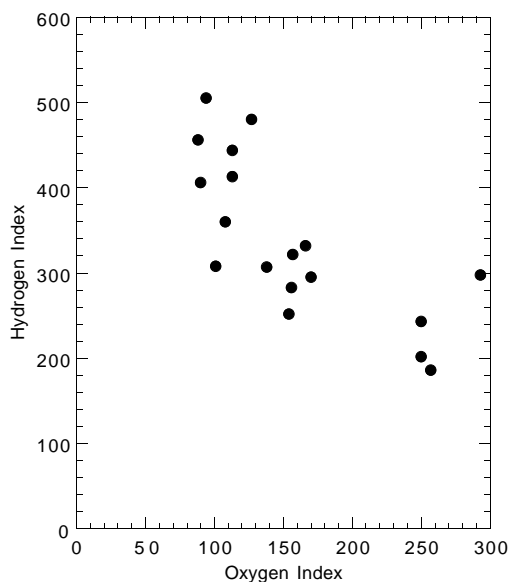


Figure 19. Rock-Eval Van Krevelen-type diagram of sediments from Hole 1083A. Organic matter appears to be type II algal material that has been variably oxidized. HI = milligrams of hydrocarbons per gram of organic carbon; OI = milligrams of CO<sub>2</sub> per gram of organic carbon.

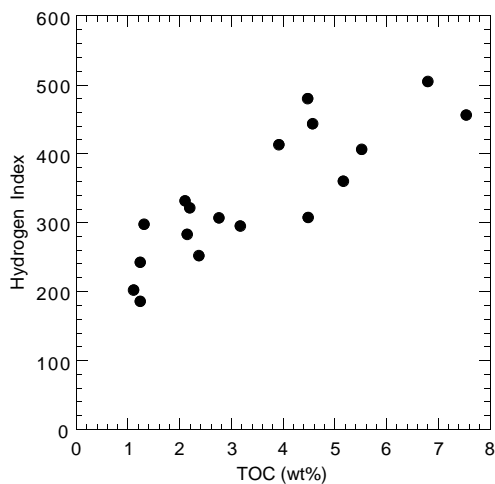


Figure 20. Comparison of Rock-Eval HI values and TOC concentrations of sediments from Hole 1083A. The correspondence between increases in both parameters indicates that preservation of marine organic matter is important to enhancing the organic carbon richness of sediments near the Walvis Ridge.

**Table 12. Results of Rock-Eval pyrolysis analyses of sediments from Hole 1083A.**

Core, section, interval (cm)	Depth (mbsf)	TOC (wt%)	S <sub>1</sub>	S <sub>2</sub>	S <sub>3</sub>	T <sub>max</sub> (°C)	HI	OI
175-1083A-								
2H-1, 46-47	2.26	3.17	1.72	9.37	5.41	411	295	170
3H-3, 46-47	14.76	4.47	1.58	21.48	5.69	420	480	127
7H-4, 46-47	54.16	4.57	1.84	20.33	5.20	411	444	113
8H-4, 45-46	63.65	6.80	3.98	34.38	6.42	400	505	94
14H-4, 45-46	120.75	4.48	1.00	13.80	4.53	409	308	101
15H-6, 45-46	133.15	7.54	1.92	34.43	6.67	404	456	88
17H-4, 45-46	149.25	5.17	1.12	18.62	5.62	412	360	108
20H-2, 46-47	174.76	1.31	0.31	3.91	3.84	414	298	293
20H-4, 46-47	177.76	1.23	0.23	2.29	3.17	411	186	257
20H-5, 60-61	179.40	1.23	0.42	3.00	3.08	407	243	250
20H-5, 100-101	179.80	1.11	0.22	2.25	2.78	409	202	250
20H-5, 144-145	180.24	2.14	0.49	6.07	3.35	409	283	156
20H-6, 4-5	180.34	2.19	0.51	7.07	3.46	410	322	157
20H-6, 46-47	180.76	2.10	0.52	6.98	3.49	409	332	166
20H-6, 80-81	181.10	5.52	1.83	22.44	5.02	400	406	90
20H-6, 144-145	181.74	3.92	1.19	16.21	4.46	408	413	113
20H-7, 19-20	181.99	2.76	0.70	8.50	3.82	410	307	138
20H-7, 60-61	182.40	2.37	0.42	5.99	3.65	411	252	154

Notes: TOC = total organic carbon; HI = hydrogen index; and OI = oxygen index. Units of the various Rock-Eval parameters are given in the "Organic Geochemistry" section of the "Explanatory Notes" chapter (this volume).

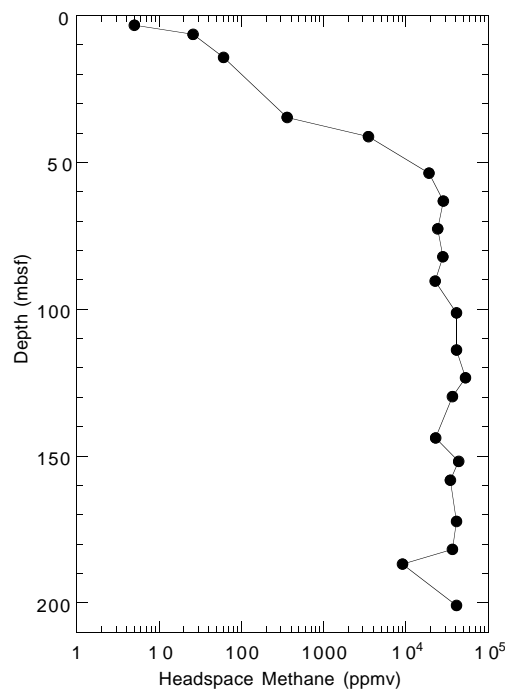


Figure 21. Headspace methane concentrations in sediments from Hole 1083A.

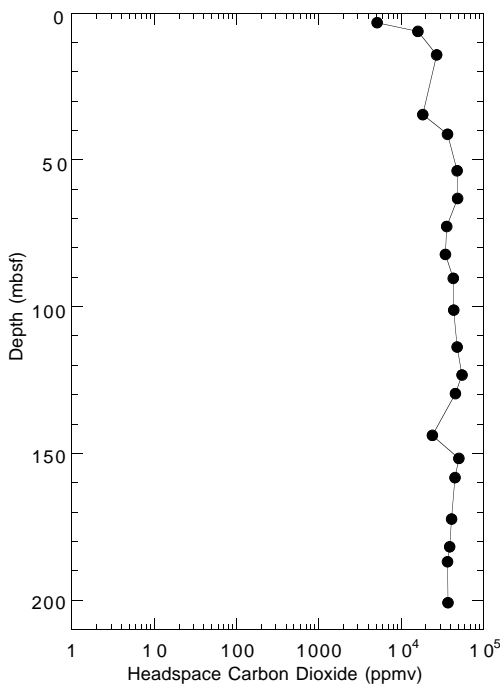


Figure 22. Headspace CO<sub>2</sub> concentrations in sediments from Hole 1083A.

**Table 13. Results of headspace gas analyses of sediments from Hole 1083A.**

Core, section, interval (cm)	Depth (mbsf)	C <sub>1</sub> (ppmv)	CO <sub>2</sub> (ppmv)	C <sub>2</sub> = (ppmv)	C <sub>2</sub> (ppmv)	C <sub>3</sub> (ppmv)	C <sub>1</sub> /C <sub>2</sub>
175-1083A-							
2H-2, 0-5	3.30	5	5,121				
2H-4, 0-5	6.30	26	16,071	0.2			
3H-3, 0-5	14.30	61	27,113				
5H-4, 0-5	34.70	361	18,293		0.3		1,203
6H-2, 0-5	41.30	3,515	36,497		0.6		5,858
7H-4, 0-5	53.70	19,076	48,028	0.2	1.6		11,923
8H-4, 0-5	63.20	28,291	48,559		2.1		13,472
9H-4, 0-5	72.70	24,252	36,067		1.4		17,323
10H-4, 0-5	82.20	28,051	34,555		1.4		20,036
11H-3, 0-5	90.38	22,643	42,886	0.2	1.8		12,579
12H-4, 0-5	101.20	40,802	43,449		2.3		17,740
13H-6, 0-5	113.80	40,947	47,847		3.5	2.0	11,699
14H-6, 0-5	123.30	52,926	54,602	0.2	3.7	1.8	14,304
15H-4, 0-5	129.70	36,787	45,559	0.3	2.9	1.1	12,685
16H-7, 0-5	143.80	22,873	24,091		1.5	0.6	15,249
17H-6, 0-5	151.80	43,376	50,258		3.6	1.7	12,049
18H-4, 0-5	158.20	34,566	45,254	0.2	2.7	0.9	12,802
19H-7, 0-5	172.30	41,007	40,885	0.7	3.1	1.1	13,228
20H-7, 0-5	181.80	36,912	38,956	0.2	3.5	2.0	10,546
21H-4, 0-5	186.80	9,063	36,686		1.0	0.5	9,063
22H-7, 0-5	200.80	40,915	37,008	0.2	3.4	1.6	12,034

Notes: C<sub>1</sub> = methane; CO<sub>2</sub> = carbon dioxide; C<sub>2</sub>= = ethene; C<sub>2</sub> = ethane; and C<sub>3</sub> = propane. Dominance of C<sub>1</sub> over C<sub>2</sub> indicates that the gases originate from in situ microbial degradation of organic matter.

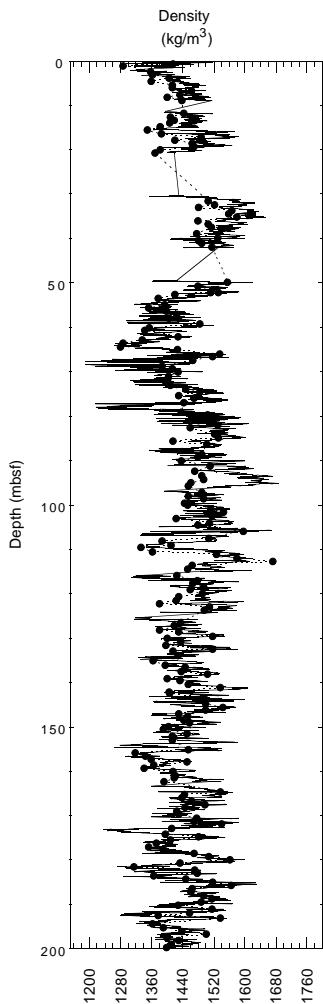


Figure 23. Gravimetric wet bulk density values (solid circles) compared with GRAPE density data (solid line) at Hole 1083A.

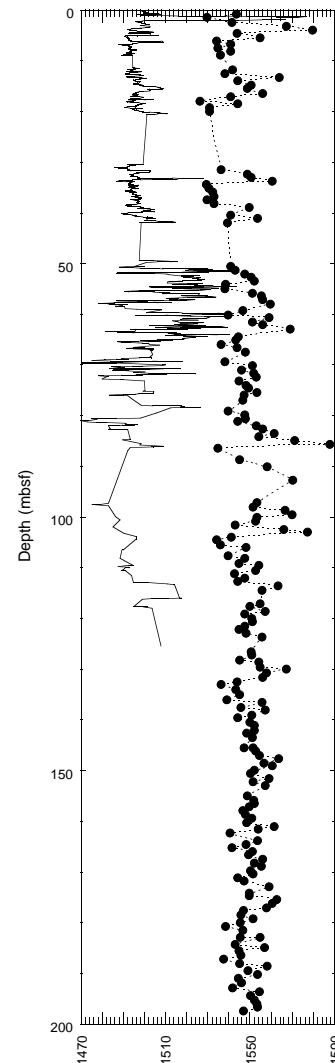


Figure 24. Discrete velocity profile (solid circles) compared with MST P-wave velocities (solid line) measured at Hole 1083A.

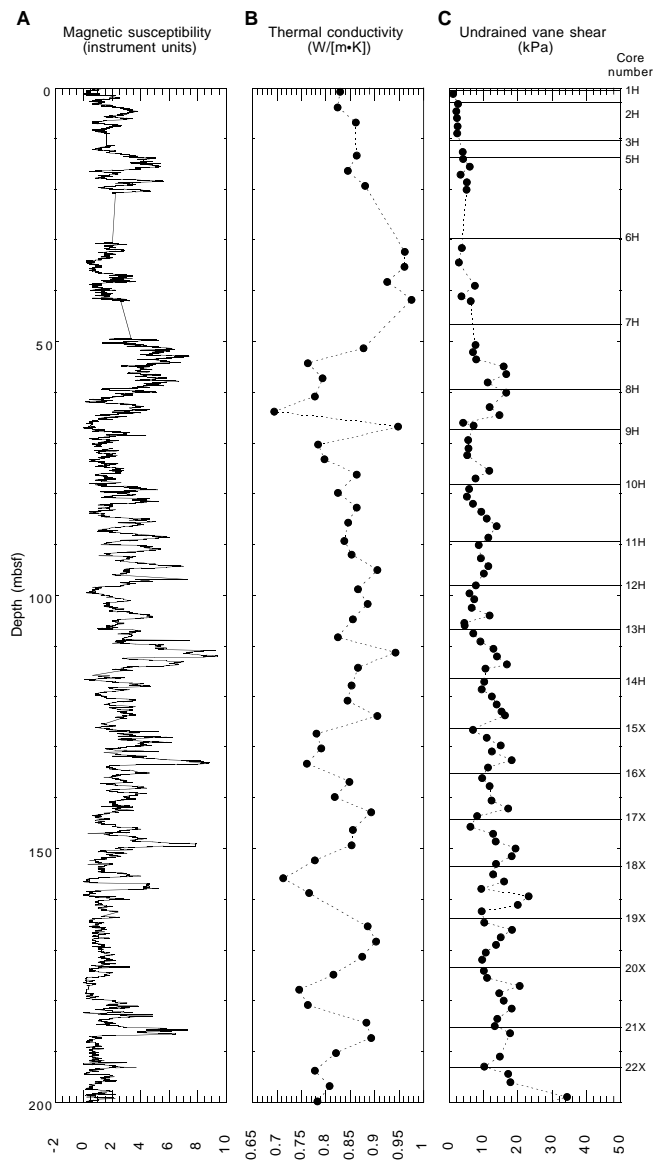


Figure 25. Plots of (A) magnetic susceptibility from MST measurements compared with discrete values of (B) thermal conductivity and (C) undrained vane shear strength between 0 and 200 mbsf for Hole 1083A.

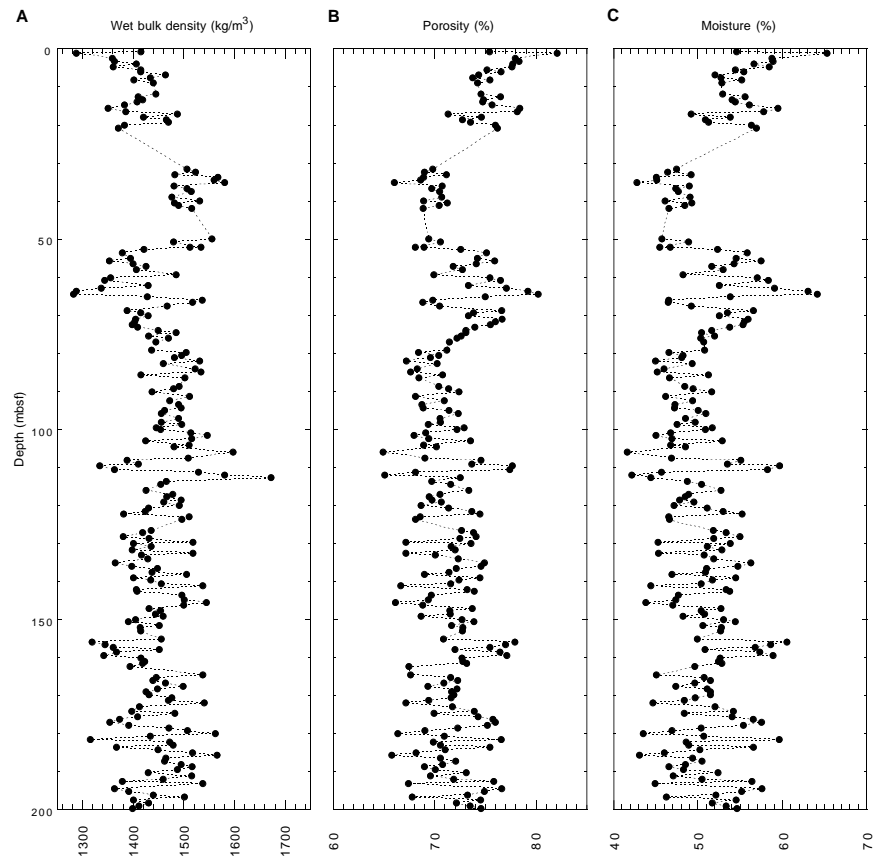


Figure 26. Gravimetric (A) wet bulk density, (B) porosity, and (C) moisture content derived from index properties measurements for Hole 1083A.